SYNTHESIS OF $Ag:SiO_2:Ag$ CORE:SPACER:SHELL NANOPARTICLES VIA THE HYDROGEN REDUCTION METHOD AND THE CHARACTERIZATION OF THEIR OPTICAL PROPERTIES

A thesis presented to the faculty of the Graduate School of
Western Carolina University in partial fulfillment of the
requirements for the degree of Master of Science in Chemistry.

By

James Parker Cook

Director: Dr. David D. Evanoff, Jr.
Assistant Professor of Chemistry
Department of Chemistry & Physics

Committee Members: Dr. Carmen L. Huffman, Chemistry
Dr. Channa R. De Silva, Chemistry

March 2014

TABLE OF CONTENTS

LIST OF TABLES

LIST OF FIGURES

LIST OF ABBREVIATIONS

$(d\sigma_{RS}/d\Omega)_{ref}$	-absolute differential cross section of the reference standard
$(d\sigma_{RS}/d\Omega)_{samp}$	-absolute differential cross section of a non-SERS dye sample
$(d\sigma_{RS}/d\Omega)_{SERS}$	-absolute differential cross section of a SERS dye sample
AEF	- analytical enhancement factor
Ag	- silver
$Ag:SiO_2$	- silver:silica core:shell nanoparticle
$Ag:SiO_2:Ag$	- silver:silica:silver core:spacer:shell nanoparticle
APTMS	- (3-aminopropyl)trimethoxysilane
arb. U.	- arbitrary units
b	- pathlength
BMP	- 2-bromo-2-methylpropane (reference standard for EF measurements)
BTA	- benzotriazole
C_{ref}	- molar concentration of dye of the reference standard
C_{samp}	- molar concentration of dye of a non-SERS sample
C_{SERS}	- molar concentration of dye of a SERS sample
CSS	- core:spacer:shell particle
CV	- crystal violet
EAS	- extinction, absorption, and scattering
EASeff	- extinction, absorption, and scattering efficiencies
$I(x)$	- Intensity profile function
ICP-OES	- inductively coupled plasma optical emission spectroscopy
I_{max}	- maximum intensity of Raman active substrate
I_{ref}	- area under a particular Raman band of the reference standard
I_{samp}	- area under a particular Raman band of a non-SERS sample
I_{SERS}	- area under a particular Raman band of a SERS sample
ITO	- indium tin oxide
NA	- numerical aperture
n	- number of particles per milliliter
OD	- optical density
PVP	- poly(4-vinylpyridine)
R6G	- rhodamine 6G
SEM	- scanning electron microscopy
SERS	- surface enhanced Raman spectroscopy
SiO_2	- silicon dioxide (silica)
$SiO_2:Ag$	- silica:silver core:shell nanoparticle
SMEF	- single molecule enhancement factor
SPPR	- surface plasmon polariton resonance
STEM	- scanning transmission electron microscopy
TEOS	- tetraethoxysilane
TMOS	- tetramethoxysilane
UV-Vis	- ultraviolet-visible spectroscopy

w_0 - laser beam waist
x - the current position of the laser beam
x_0 - the position of the cleaved edge of the silicon wafer
$\varepsilon_1(\omega)$ - real component of the dielectric function of silver
$\varepsilon_2(\omega)$ - imaginary component of the dielectric function of silver
σ_{exe} - extinction cross section

ABSTRACT

SYNTHESIS OF Ag:SiO_2:Ag CORE:SPACER:SHELL NANOPARTICLES VIA THE HYDROGEN REDUCTION METHOD AND THE CHARACTERIZATION OF THEIR OPTICAL PROPERTIES.

James Parker Cook, M.S.

Western Carolina University (March 2014)

Director: Dr. David D. Evanoff, Jr., Ph.D.

Plasmonic nanostructures are of considerable interest due to their unique mechanism for light interaction and the considerable number of applications that result from, or are enhanced by, these interactions. Extensive work has been reported on the synthesis, modeling, and utilization of various morphologies of plasmonic structures. As such, there is an increasing need to better define the optical properties of these materials to better understand and refine current theories in order to adapt to future applications.

Herein the synthesis of Ag:SiO_2:Ag core:spacer:shell (CSS) nanoparticles of varying geometries is reported. CSS synthesis utilizes an adaptation of the hydrogen reduction method and results in highly crystalline particles free of surface-modifying groups. This is advantageous as any molecule on the surface of the particle will influence the plasmonic properties. Extinction efficiencies of the composite CSS particles as well as the effect of varying shell and spacer thicknesses on the relative ratio of the scattering and absorptive plasmon relaxation modes are reported. Likewise, the relationship between CSS particle geometry and surface enhanced Raman spectroscopy (SERS) enhancement factor is explored.

CHAPTER 1. BACKGROUND

Plasmonics is an emerging field within the area of materials chemistry with applications spreading through all fields of the scientific community including biological imaging, single molecule detection, instrumental design, medicinal applications, and photovoltaic applications.[1–5] Extensive research has been published on synthesis, analysis, and applications of plasmonic nanoparticles within the various fields of science.[6,7] One reason for the interest in nanomaterials is the unique properties that arise when certain materials become nanoscopic. Silver and gold nanoparticles, on the order of 100 nm scatter light with remarkable efficiency and are useful for targeting cancer cells.[1] Gold nanoparticles have been reported to effectively kill cancer cells through photothermal absorption.[5] Colloidal aggregates of silver and/or gold are often used as substrates for Raman and fluorescence spectroscopy to increase the analyte signal.[8–10] These unique optical properties arise from the confinement of the nanoparticle's electrons to an area much smaller than the wavelength of light that is used to probe the system.[11]

1.1. Introduction to plasmonics

Metallic nanoparticles of suitable dimensions all exhibit a surface plasmon polariton resonance (SPPR), which is the collective oscillation of the free conduction electrons. Noble metal nanoparticles have particularly strong SPPRs as they have many free conduction electrons. Likewise, unlike any other metal, the noble metals have SPPRs that appear in the visible spectral region. Silver nanoparticles are particularly of interest for several reasons. First, unlike gold and copper, which display a color, silver has no inter-band transitions in the visible region meaning any interaction with visible

light is due to the plasmon resonance. Second, silver metal donates about one electron per atom to the conduction band, more than copper or gold. Third, silver is significantly less expensive than gold. There are, however, some issues that make silver less attractive to the scientific community. The most prevalent is that silver is significantly more reactive than gold, such that many researchers choose gold for the ease of synthesis.

From here on, all discussion of nanoparticles and the associated plasmons, unless otherwise stated, will be in the context of silver particles, though the same theory applies to the other metals as well. The SPPR process can be described in two events, (1) excitation through the absorption of a photon and (2) dissipation of energy, either through resonant scattering or through interaction with lattice phonon modes, resulting in the heating of the surrounding medium.[11]

1.1.1. Absorption of light

The plasmon of a silver particle is governed by the acceleration of conduction electrons by the electric field of incident radiation, the restoring force in the particle, and the confinement of electrons to dimensions less than the wavelength of light that is impingent upon the surface of the particle.[11] As light impinges on the surface of the particle, the photon is annihilated and 100 % of the energy of the photon is transferred to the particle, displacing the delocalized electrons from their homeostatic positions, polarizing the particle. The particle's conduction electrons will oscillate with the same frequency as the photon that was absorbed.

As the electrons move to one side of the particle, a restoring force is induced from the electron deficient metal lattice, opposing the acceleration of the electrons. The restoring force increases as the displacement of the electrons increases until the restoring

force is strong enough to change the direction of the electrons. At this point the electrons are accelerated to the opposite side of the particle where the whole process is repeated. This restoring force is influenced by the local medium surrounding the outside of the particle. The more polarizable the medium, or the higher refractive index, the more the solvent is polarized which reduces the restoring force. This effect can be demonstrated as a silver particle is coated in a layer of silicon dioxide (silica or SiO_2) dispersed in water. In coating the particle there is a red-shift in the extinction spectrum as the silica layer has a higher refractive index than water.[12] The decreased restoring force causes the resonant oscillation frequency to decrease.

The last factor that influences the SPPR explains different resonant modes observed from the interaction of the nanoparticle with light in the visible spectrum. The resonant modes describe the "path" the electrons take in their oscillations. These resonances were first explained by Gustav Mie in 1908 through his solutions for Maxwell's equations. In this paper Mie provided illustrations describing the electric fields generated during resonant modes (Figure 1 A-C).[13] A dipole resonance (C) is the simplest resonant mode in which the electrons only oscillate parallel to the direction of the electric field of incoming radiation. Examples of the quadrupole (B) and octupole (A) resonances of the particles are also shown where the electrons oscillate in more complex patterns. These modes all exist during a SPPR, however the relative ratios of these resonances change as the particle increases in size. Small particles tend to be dominated by a dipole resonance, as the wavelength of the light is much greater than the diameter of the particle. This resonance can be explained visually by viewing the particle in relation to an electric field of a photon. In Figure 1D, not drawn to scale, a small

particle is shown to experience a uniform electric field a majority of the time while a larger particle spends much more time in opposing electric fields during the course of an oscillation. These opposing electric fields give rise to the more complicated resonant modes.

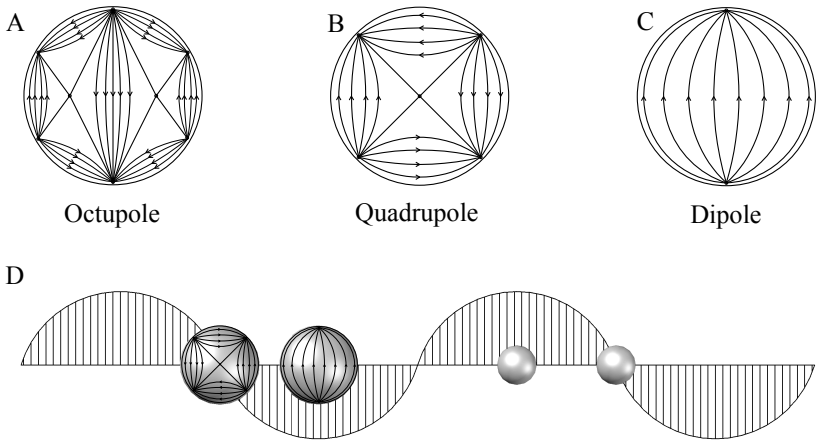

Figure 1. Diagram of plasmon resonance modes (A). A representative electric field plotted with two sets of silver particles (B).

In an ultraviolet-visible (UV-Vis) spectrum of a colloidal suspension, as the diameter of the particles increase in size it is possible to see strong extinction bands, the combination of absorption and scattering, that correspond to the various resonant modes. Figure 2 shows a plot of a single colloidal synthesis with aliquots taken at constant intervals during the course of the reaction. In this type of reaction, which will be discussed in Section 1.2.2.3, the concentration of suspended particles remains constant and the particle diameter is directly proportional to the reaction time. The increase in overall extinction of the particles is due to a stronger interaction with light. In the smallest spectrum, particles ca. 15 nm diameter, only a dipole resonance can be seen. The other resonances are still present but the particle is dominated by this resonance, as it

is more efficient for small particles. As the diameter increases the dipole resonance red shifts, uncovering the quadrupole resonance. The quadrupole also shifts but more slowly in relation to the dipole resonance. The red shift in the plasmon is also related to the increasing diameter of the particles as the free conduction electrons now have a larger distance to travel, and perhaps more importantly the increased surface area of the particle allows for a stronger solvent interaction with the metal lattice, reducing the restoring force in the particle. The quadrupole is less sensitive to the solvent interactions as the surface area increase is less significant with the more complex resonances.

The quadrupole also becomes more prominent as a result of the size increase. The quadrupole is more probable at higher frequency resonances as a particle of larger size spends more time in opposing electric fields compared to smaller particles. It is perhaps easiest to illustrate this by referring to Figure 1D where two particles are shown on top of a representation of the electric field of light. For the small particle in the figure, the dipole resonance is more probable because it is mostly influenced by a uniform electric field. At this same frequency, the large particle in the figure would exhibit a higher order resonance mode as most of the time it experiences opposing electric fields.

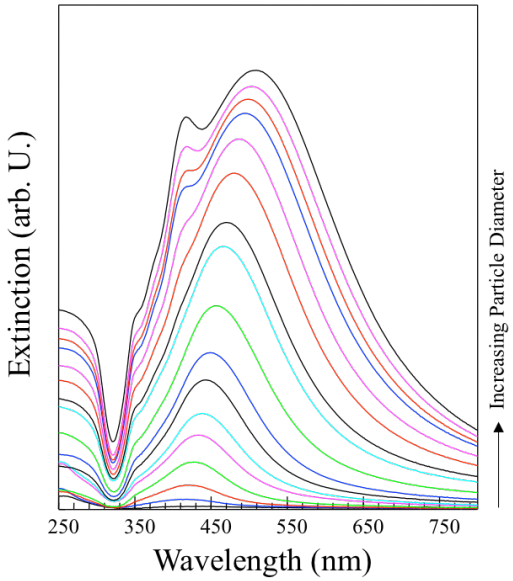

Figure 2. Plot of plasmon resonance as the diameter of the nanoparticles in a colloidal suspension is increased.

1.1.2. Dissipation of energy

Silver particles release the energy from an SPPR excitation in one of two ways: (1) dissipating the energy to the surrounding medium as heat, or (2) scattering a photon of the same wavelength as the one that was annihilated. Using an integrating sphere, it is possible to extract the scattering and absorption components of a suspension of particles, described in detail in Section 3.4. Separating the scattering and absorption components allows one to see how these ratios change as a result of particle diameter. It has been shown experimentally that as particle diameter increases, the plasmon peaks (dipole, quadrupole etc.) will slowly red shift due to the aforementioned decrease in restoring force, and the scattering to absorption ratio will also change.[14] Small particles with diameters less than ~40 nm have very low scattering while larger particles of diameter greater than ~90 nm have very high scattering.[14] This change in scattering and absorption

ratios can best be explained by examining the real and imaginary components of silvers dielectric function.

As seen in the 1972 paper of Johnston and Christi,[15] the imaginary component $\varepsilon_2(\omega)$, which controls absorption, remains constant throughout the visible spectrum. The magnitude of the real component of the dielectric function, $\varepsilon_1(\omega)$, which governs the resonant scattering relaxation pathway, increases sharply as wavelength increases across the visible spectrum.[15] As the plasmon resonance red shifts due to the decreased restoring force of the particles, the scattering component of the plasmon increases as the plasmon band is shifted out to longer wavelengths. Essentially one can tune the optical properties desired for an experiment just by changing the particle diameter.

1.2. Nanoparticle synthesis

There are many different methods for creating silver nanoparticles, with varying benefits for each method. Some things to consider when looking at properties of suspensions are the average size of each particle, distribution of particle size, the reproducibility of the reaction, and the morphology of the particle (spheres, rods, cubes, crystalline, shells).[5,16,17] The application of the particles often determines the method used for synthesis, nevertheless a brief discussion of several methods is presented to help illustrate the direction from which this research originated.

1.2.1. Stöber method (silica synthesis)

The first synthesis of nanoparticles discussed here illustrates basic preparation of silica or glass nanoparticles (SiO_2). This method was first reported by Werner Stöber in the late 1960's.[18] This reaction is used to make both silica nanoparticles and to coat silver nanoparticles with a layer of glass. Regardless of the synthetic goals of the system

the basic reactions are essentially the same. The synthesis follows a simple two-step reaction of hydrolysis (1) of some species of tetra-alkoxysilane ($Si(OR)_4$), followed by a condensation reaction (2), catalyzed by ammonium hydroxide (NH_4OH).[18]

$$Si(OR)_4(l) + 4H_2O(l) \xrightarrow[\text{cat. } NH_4OH]{\text{2-propanol}} Si(OH)_4(l) + 4HOR(l) \quad \textbf{(1)}$$

$$2Si(OH)_4(l) \xrightarrow[\text{cat. } NH_4OH]{\text{2-propanol}} (OH)_3Si\text{-}O\text{-}Si(OH)_3 + H_2O(l) \quad \textbf{(2)}$$

This condensation results in dense aggregates of cross-linked silanes. Eventually the small aggregates of silanes are linked together as they either accumulate on the surface of a silver particle, or form independent silica nanoparticles. The condensation step in this reaction can be catalyzed by acid or base. The acid catalyzed method forms a less porous (more dense) network of silica,[19] which would be more desirable for this study as a more dense layer of silica would present a more homogenous glass matrix. However the HCl severely etch the silver particles in suspension before condensation. As such, the base catalyzed method is employed to avoid extensive etching of the silver particles.

1.2.2. Silver nanoparticles (synthesis)

1.2.2.1. Lee-Meisel method (trisodium citrate reduction)

This method of silver particle synthesis involves the reduction of silver nitrate ($AgNO_3$) with trisodium citrate (1 % solution).[20] The resulting particles are polydispersed with a diameter of ca. 60 nm and have a citrate coating on the outside of the particles. This protects the particles from contaminants making them more resistant to aggregation than unprotected particles. The surface modifying groups will affect the plasmon resonance, and the polydispersity of the colloid may be undesirable depending on the application.

1.2.2.2. Creighton method (sodium borohydride reduction)

This method of silver particle synthesis uses $AgNO_3$ as the silver species but uses sodium borohydride ($NaBH_4$) as the reducing agent.[21] This method can produce a monodispersed colloid of about 10 nm and the particle surfaces are protected by borates in the suspension. The narrow size distribution of the particles is desirable, however, the small size of the particles may limit the application scope of the particles.

1.2.2.3. Hydrogen reduction method

The hydrogen reduction method utilizes silver (I) oxide (Ag_2O) as the silver species and hydrogen (H_2) gas as the reducing agent. Dissolved H_2(g) reduces the aqueous silver (I) oxide species yielding silver metal and water as the products.[22] The net chemical reaction is shown as

$$Ag_2O(aq) + H_2(g) \xrightarrow[10\ psi]{70^\circ C} Ag^0(s) + H_2O(l) \quad \textbf{(3)}$$

The slow growth of the silver particles results in a highly crystalline, monodispersed suspension of silver particles that have no surfactants and no ionic species other than the silver species resulting from the Ag_2O solubility. The relatively low K_{sp} for Ag_2O(s) is key to the effectiveness of this reaction. Throughout the course of the reaction, the solution contains a constant concentration of silver species due to saturation. The solubility of each silver species is shown in Equations 4-6.[23]

$$\tfrac{1}{2}Ag_2O(aq) + \tfrac{1}{2}H_2O(l) \rightarrow Ag^+(aq) + OH^-(aq) \quad K_{S0} = 1.9x10^{-8} \quad \textbf{(4)}$$

$$\tfrac{1}{2}Ag_2O(aq) + \tfrac{1}{2}H_2O(l) \rightarrow AgOH(aq) \quad K_{S1} = 2x10^{-6} \quad \textbf{(5)}$$

$$\tfrac{1}{2}Ag_2O(aq) + \tfrac{1}{2}H_2O(l) + OH^-(aq) \rightarrow Ag(OH)_2^-(aq) \quad K_{S2} = 1.9x10^{-4} \quad \textbf{(6)}$$

These suspensions are unique in that they are bare silver particles with only the silver oxide species occupying the hydration shell of the particles. The diameter of the particles in suspension is proportional to the time the reduction is allowed to proceed, so this method can easily produce any monodispersed colloid of silver in a specific diameter with no further optimization of the reaction conditions.[22] One downfall of this method is that silver rods and plates are created along with the spherical nanoparticles so the suspension must be filtered to reduce the concentration of these other morphologies such that the overall plasmon resonance of the suspension is not affected.

The hydrogen reduction reaction does not proceed efficiently in a quartz vessel; this curious result suggests that the reaction is catalyzed by ions in the walls of the Pyrex® vessel. It is hypothesized that the ions in the walls of the Pyrex® vessel help to initiate particle nucleation that continues to grow from the continued reduction of Ag^+ forming highly crystalline silver particles suspended in water.

1.2.3. Silver shells

There are currently several methods for creating SiO_2:Ag core:shell particles. All of theses methods involve some silica surface that is decorated with either silver or gold particles, which act as nucleation sites for the growth of silver or gold shells. Prior to decoration, silica surfaces must be treated to facilitate particle attachment. The most common method utilizes (3-aminopropyl)trimethoxysilane (APTMS) which, reacts under the same conditions as a Stöber reaction to decorate the surface of silica particles with a primary amine group. Very small gold particles, 1-3 nm, are added to the suspension of functionalized silica and the gold is adsorbed to the lone pair of electrons on the amine group. Silica surfaces can also be treated by exposure to tin (II) chloride ($SnCl_2$), which

causes Sn^{2+} ions to be adsorbed to the silica surface. Exposure of the tin-treated silica to Ag^{+} causes reduction of silver, which is bound to the surface of the silica, most likely due to electrostatic interactions.

These methods for synthesis of SiO_2:Ag particles include the reduction of silver salts to the decorated silica surface as it serves as an anchor where the newly reduced silver can accumulate without significant nucleation of additional particles in the suspension. As all of these methods involve decorated silica, coated with either silver or gold; the main difference between these procedures is the method by which silver is reduced. A procedure adapted from a silver deposition method reported by Danscher, involves the reduction of silver lactate by hydroquinone in a citrate buffer solution containing Acacia.[24,25] The SiO_2:Ag particles created by this method have rough shells characterized by large needle-like masses of silver that extend out from the surface of the particle.[25]

A second deposition method reported by Burry utilizes silver nitrate, *n*-propyl gallate, and ammonium hydroxide to deposit silver onto the decorated surface of the silica.[25,26] This method produces rough shells that resemble colloidal aggregates that have accumulated on the surface of the particle as well as the growth some independent silver particles in the reaction suspension.[25] The asymmetric shape of SiO_2:Ag particles produced from the first method and the extra colloidal particles resulting from the second method would make characterization of the suspensions, both physically and theoretically, very difficult.

The third method for producing SiO_2:Ag particles solves several of the problems inherent in the last two methods. It involves the reduction of silver nitrate with

formaldehyde and NH_4OH.[25] The rapid change in pH results in the reduction of silver ions in solution where they subsequently adhere to the decorated silica surface. This results in the formation of smooth silver shells that are uniform in appearance with no apparent growth of colloidal silver in solution.

A fourth method involves decorating the silica with the aforementioned $SnCl_2$ and allowing the Sn^{2+} to reduce ammoniacal silver nitrate (Tollens' reagent) via a redox reaction.[27] The particles are centrifuged several times before being placed in more of the Tollens' reagent with formaldehyde, which serves as the reducing agent, creating a dense uniform shell.[27] All of these methods are proven to work, however all have species in solution and on the particle's surface that will affect the plasmon resonance and most likely the lifetime of the suspension. With that in mind, it would be desirable to produce silver shells via a chemically clean pathway whilst maintaining the symmetric morphology and the absence of independent silver particles from the suspension.

1.3. Particle-particle interactions

In addition to the single particle plasmons that were previously discussed, collective plasmons of 2 or more proximal particles can be observed. Plasmon coupling has been shown experimentally in a study where a 2-dimensional array of ca. 100 nm silver nanoparticles was produced in a film of poly (dimethylsiloxane).[28] UV-Vis spectra were taken as the film was stretched in two dimensions. While the particles were close to each other, the film exhibited a Lorentzian-like extinction spectrum whose maximum corresponded to the quadrupole resonance of uncoupled particles. As the film was stretched the extinction spectrum eventually resembled that of uncoupled particles in suspension. Coupling is the result of the interaction of the local electromagnetic fields

that extend away from the surface of particles undergoing SPPR excitation (Figure 3A). This experiment shows that plasmonic particles couple as a function of decreasing interparticle distance.[28] A result of particle coupling is that the electromagnetic field between the particles is much stronger than that of uncoupled particles (Figure 3B).[29]

Though plasmon oscillations involve the oscillation of all the free conduction electrons in a particle, the effects of the plasmon are only manifested at the surface of the particle as that is where charge neutrality is broken. When two particles' plasmon modes are coupling, it is the two surfaces of the particles that are interacting to produce the intense electric field. This gives way to an interesting effect in SiO_2:Ag particles in which there is a silver shell on top of a dielectric core particle, such as silica (Figure 3C).[6] In this case, coupling occurs within each particle as the outer-shell surface will couple to the inner shell surface causing an enhancement in the electric field. One could go a step further and consider a Ag:SiO_2:Ag core:spacer:shell particle (CSS) in which the core is silver, the spacer is silica, and the shell is silver (Figure 3D).[6] In this scenario, there are three surfaces that should be accounted for, which through coupling could produce a strong electric field.

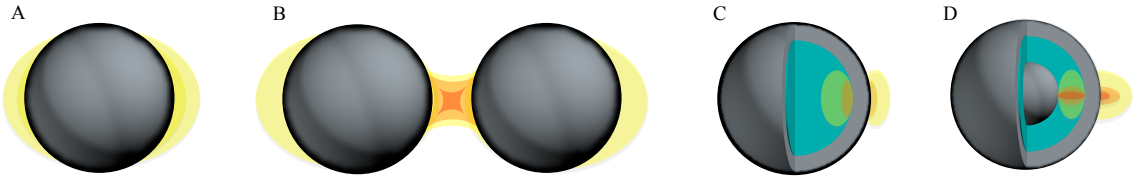

Figure 3. Silver nanoparticles showing the electric field (yellow). The coupled nanoparticles display a much stronger electric field (dark-yellow/orange). Particle (A) shows the electric field of a solid particle, (B) shows the electric field between coupled nanoparticles, (C) shows a SiO_2:Ag particle, and (D) shows as CSS particle with a high level of coupling.

1.4. Raman scattering

Raman scattering is a type of vibrational spectroscopy that utilizes lasers to probe a system. A Jablonski diagram[30] (Figure 4) can be used to illustrate a Raman scattering event. In the diagram, S_0 is the ground electronic state of a molecule and the $V_{0\text{-}4}$ are the vibrational states of the molecule within that electronic state. S_1 is the first excited state of the molecule and T_1 is the triplet state of the molecule. Raman scattering is the result of a photon promoting an electron to a virtual state followed by immediate reemission of energy. The electron falls back to a ground state energy level and emits a photon of slightly more or less energy, anti-stokes- or stokes-shifted respectively, than what was first absorbed. The energy difference between the laser source and the scattered light (Raman) detected is indicative of the energy lost or gained through bond vibrations within the molecule. A vast majority of the light is scattered back at the same energy (Rayleigh) of the light that was used to probe the molecule. Raman scattering is a very rare event that is difficult to measure in low concentrations. However, since Raman-active molecules have unique Raman spectrum, and water has a very low Raman cross

section, it is a valuable spectroscopy technique that has gained considerable interest in recent years.

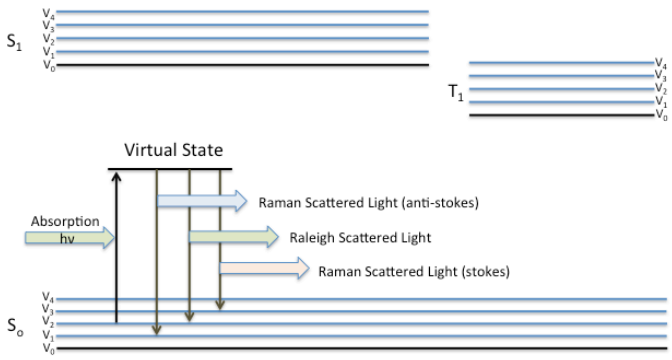

Figure 4. Jablonski diagram demonstrating Raman scattering.

1.5. Surface enhanced Raman scattering (SERS)

Silver substrates serve as great surfaces to measure Raman scattering. The phenomenon was first reported in 1974 using pyridine adsorbed to roughened silver electrodes.[31] Silver particles were later discovered to exhibit strong enhancement of Raman signal with colloidal aggregates exhibiting an increase in Raman signal of several orders of magnitude.[20] The use of substrates, regardless of the composition or morphology, is known as surface enhanced Raman spectroscopy (SERS). This enhancement is, in part, the result of an increase in the analyte's polarizability due to the influence of the local plasmonic electric field. Likewise, resonant scattering by the particle causes an increase in the field strength of the incoming radiation near the particle surface thereby increasing the probability of a Raman scattering event.

It has since been reported that this enhancement in Raman signal occurs when a molecule is in the gap between two particles that are coupled together. This position has been since labeled as a "hot spot" for Raman enhancement and is the result of a strong

electric field that is produced between the coupled particles (cf. Figure 3B).[32] The most common way to produce SERS measurements is through the induced aggregation of silver particles using a salt such as potassium chloride (KCl). The aggregation process is somewhat controllable however the suspension is inherently unstable and will eventually collapse, complicating the quantification of the enhancement of these systems across different measurements. Aggregation is inherently heterogeneous within one suspension and among different suspensions making it difficult to compare the results of different SERS measurements. Likewise, there is a low probability that an analyte molecule will be trapped in a hot spot within the aggregate.

All of this amounts to several inherent problems with using colloidal aggregates as SERS substrates for analytical techniques. It is difficult to quantitatively measure analyte concentrations using SERS as colloidal aggregates will vary with each measurement, and the amount of time the measurement is allowed to proceed. It is also difficult to predict how many molecules will be in a hot spot when measurements are taken. It would be desirable to have a particle that could be reliably synthesized that contains the stability of a non-aggregated suspension but has the enhancement capabilities of a coupled particle without the positional constraints of a two-particle system.

CHAPTER 2. INTRODUCTION TO RESEARCH

The purpose of this research is to (1) synthesize several suspensions of CSS particles of varying geometries via the hydrogen reduction method and assess the synthetic limits for this reaction (2) observe how the CSS SPPR changes, i.e. the extinction, absorption, and scattering (EAS) cross sections and efficiencies, as the geometry of the particle changes and (3) asses their usefulness in SERS applications by determining the enhancement factor.

The first goal of this research is to define a procedure to synthesize Ag:SiO_2:Ag CSS nanoparticles. These particles will be synthesized utilizing an adaptation of the hydrogen reduction method.[22] There are several methods for building silver shells, but most use the reduction of silver salts, which results in the formation of small silver particles that aggregate around the silica surface.[25,27,33] In the hydrogen reduction method, the chemicals involved are nanopure water, silver (I) oxide, and hydrogen gas, so the matrix that the particles exist in is free from surfactants and/or surface modifying groups. This method produces silver shells that are formed as silver seeds adsorbed to the silica's surface that grow into large crystalline domains that collectively create the silver shell.

The second goal of this research is to build several sets of CSS suspensions with varying particle dimensions, analyze each suspension to find the EAS cross sections and their associated efficiencies (EASeff). To change the coupling between the Ag core and the Ag shell, the synthesis outline in Figure 5 is used, where the silver core particles will be coated with silica. This silica shell will be increased in thickness using four separate

Stöber reactions starting with the same suspensions of core particles. A silver shell will then be added to the four suspensions to make CSS particles. Also, SiO_2:Ag particles will be synthesized to compare the CSS plasmon to a silver shell plasmon.

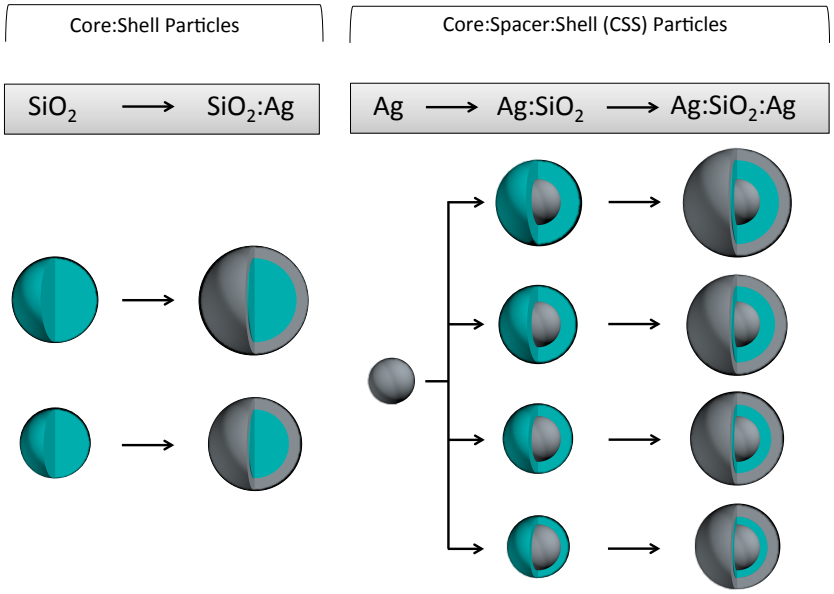

Figure 5. Proposed synthesis for core:shell and CSS particles.

Changing the spacer thickness will allow for analysis of the coupling between the silver core and silver shell and thus the absorption and scattering components of the extinction spectrum. The EASeff of the suspensions can be calculated from dividing the EAS cross section values by that of the geometric cross section of that particle,.[14] Due to a low $\varepsilon_2(\omega)$ across the visible spectrum and the freedom of the conduction electrons, silver nanoparticles have very efficient plasmon resonances, and as a result the EASeff are greater than one. There are currently reported procedures on both theory and synthesis of Au:SiO_2:Au CSS particles, which have the same structure desired for this study.[34,35] In 2011, there was a publication investigating the resonances of Ag:SiO_2:Ag

CSS particles, however no experimental data was reported.[36] Presently, no experimental data on the EASeff of silver CSS particles exist in the literature.

The third goal of this research is to test each of the particle suspensions as a SERS substrate to assess their ability to enhance Raman signal of a model analyte through calculation of the analytical enhancement factor (AEF).[37] To test this enhancement, a method that measures the enhancement from the given substrate is measured using crystal violet (CV), a dye that is a common model analyte for Raman spectroscopy. This technique utilizes a non-SERS measurement with its associated concentration to normalize the SERS measurement with its associated concentration.

Future projects can be directed from the data compiled from this study. Aforementioned suspensions will be analyzed, looking for trends that can be used to guide the next set of suspension geometries in order to optimize the geometries of particles that will exhibit the best Raman enhancement and/or the highest EASeff. Having the efficiencies of each particle diameter can allow for a more complete analysis of what type of particle geometry is best suited for SERS applications and perhaps determine if these particles are more useful than SiO_2:Ag particles or solid silver particle aggregates for repeatable SERS measurements.

CHAPTER 3. EXPERIMENTAL

3.1. Materials

ACS grade tin (II) chloride dihydrate and silver nitrate (99.9 %) were acquired from Fisher Scientific. Trisodium citrate dihydrate (99.6 %) was acquired from J.T. Baker. Silver oxide (99 %), Leuco crystal violet (99 %), rhodamine 6G (99 %), and 2-bromo-2-methylpropane (96 %) were acquired from Acrōs Organics. Benzotriazole (99 %) was acquired from Pfaltz & Bauer Inc. Tetraethoxysilane and tetramethoxysilane was acquired from Gelest. Reagent-grade absolute ethanol (>99.5 %), 2-propanol (>99.5 %), and hydrochloric acid (37.5 %) were acquired from Fisher Scientific. Water with a resistivity of 18.2MΩ was obtained from a Barnstead NANOpure Diamond system with a 0.2μm hollow fiber filter. Hydrogen gas (research grade, 99.9999 %) was received from National Specialty Gases. All chemicals were purchased and used without further purification. Fisherbrand quantitative Q5 filter paper medium porosity medium flow was purchased from Fisher Scientific. 90 mm nylon supported membranes with pore sizes of 0.45 μm, and 0.22 μm were purchased from Fisher Scientific.

3.2. Instrumentation

Particle suspensions were analyzed in an open atmosphere Agilent 8453 UV-Vis system. The shape and position of the plasmon peaks allows for assessment of reaction progress. To measure the true absorption of each suspension, a 6 inch Specralon® coated integrating sphere, purchased from Labsphere, was coupled to a Horiba LabRam HR microscope equipped with an 800 mm monochromator, 1800 groove mm^{-1} grating, and a TE-cooled CCD detector. The two systems are coupled together via a 400 μm optical

fiber exiting the integrating sphere attached to an external cuvette holder, which is then coupled to the microscope via a 100 μm optical fiber (Figure 6). The microscope, using a 10x plan achromat objective, was focused on the end of the 100 μm optical fiber then slowly adjusted to maximize the signal to the detector.

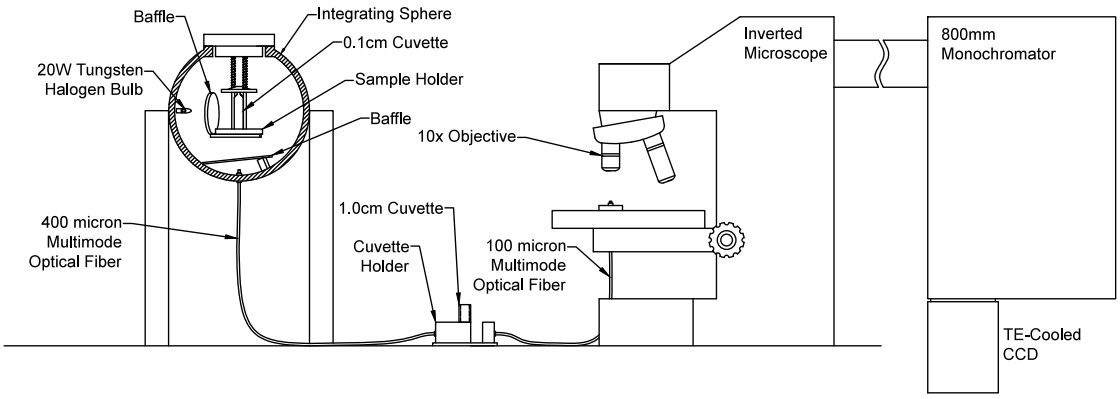

Figure 6. Diagram of the integrating sphere setup used to separate the absorption and scattering components of the extinction spectrum.

Raman scattering measurements and enhancement studies were preformed with a Horiba LabRam HR microscope equipped with an 1800 groove mm^{-1} grating and TE-cooled CCD detector, utilizing a 20 mW (7.4 mW at the sample) helium-neon (HeNe) laser with a wavelength of 632.8 nm. All Raman and SERS data was collected with a 10x infinity corrected, achromat plan objective with a numerical aperture of 0.25. Silver concentrations of colloidal suspensions were found by a series of acid digestions, which were then analyzed with a Perkin Elmer Optima 4100DV inductively coupled plasma-optical emission spectrometer (ICP-OES). A Hitachi HD 2000 scanning transmission electron microscope (STEM) operating at 200 kV and a Hitachi S-4800 scanning electron microscope (SEM) operating at 5-20 kV was employed to image suspensions. For

STEM, suspensions were drop cast on formvar-coated copper grid from Electron Microscopy Sciences.

3.3. Synthesis

In this section, the notation used to describe various Ag:SiO_2:Ag core:spacer:shell (CSS) particles will be as follows. Because the goal of this study was to create particles with similar silver shell thicknesses, differences in CSS particles occur in the silver core diameter and in the silica spacer thickness. Three colloidal suspensions of silver were prepared to serve as the cores of CSS particles and are labeled A, B, and C in order of increasing particle diameter. For each core, four independent Stöber reactions were carried out to coat the cores with silica spacer layers. Spacer layer thickness is denoted 1, 2, 3, and 4 in order of increasing thickness. Final CSS particles are denoted by their core letter and spacer number. For example, B4 CSS particles are constructed from the intermediate silver core diameter and have the thickest silica spacer layer of all the CSS particles containing 'B' cores. In Figure 7, a schematic of the naming scheme is shown with approximate dimensional values. A visual representation of the synthesis of CSS particles is given in Figure 8. This method will be described in detail in subsequent sections.

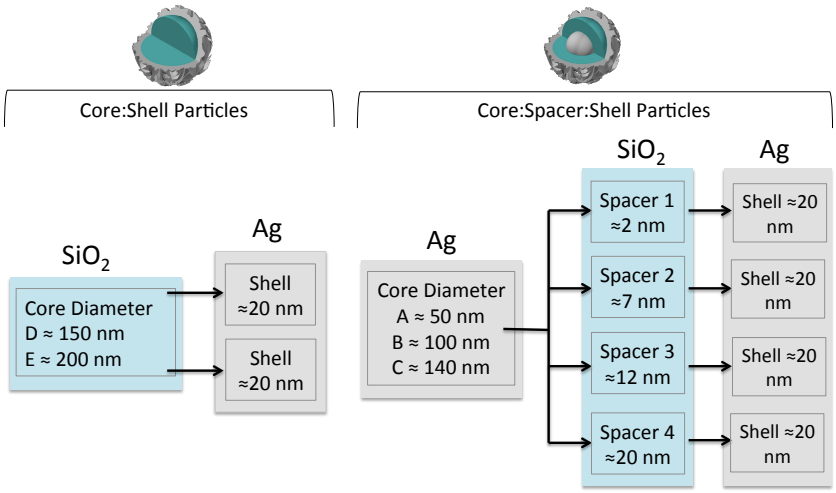

Figure 7. Schematic of the naming scheme for CSS particles. This scheme is carried throughout the rest of this discussion with the predicted values from the proposed synthesis.

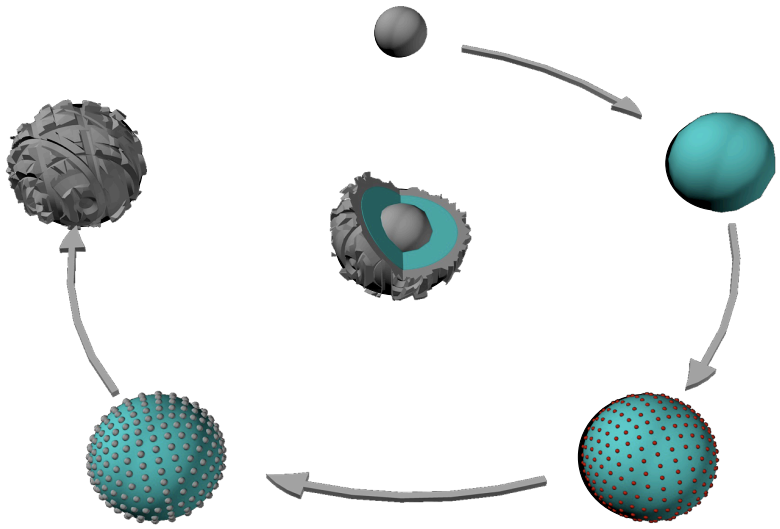

Figure 8. Schematic of CSS synthesis to be used in this document. Silver is denoted in grey, silica is blue-green, and Sn^{2+} is red.

3.3.1. Synthesis of silica particles

Two diameters of silica particles were prepared through the Stöber method in which 650 µL of tetraethoxysilane (TEOS) was added to 50 mL of absolute ethanol

followed by 2 or 3 mL of NH_4OH (30 %). The reaction was allowed to proceed at room temperature with vigorous stirring. After 24 hours, particles were washed via centrifugation with 100% ethanol, 50% ethanol:water, and nanopure water before being dispersed in 10 mL of water. One milliliter of the suspension was added to a dried weighed scintillation vial and dried in an oven to obtain a mass of silica per milliliter of suspension.

3.3.2. Synthesis of silver particles

3.3.2.1. Lee-Meisel colloid

A suspension of Lee-Meisel particles was prepared for SERS studies. A 500 mL solution of 1.06 mM $AgNO_3$ was brought to a boil under vigorous stirring. To the boiling solution of $AgNO_3$, 10 mL of a 1 % trisodium citrate solution was added dropwise and mixed for 1 hour. The suspension was then allowed to cool under gentle stirring and stored in a clean 600 mL plastic container.

3.3.2.2. Hydrogen reduction colloid

Silver nanoparticles were prepared by hydrogen reduction of silver (I) oxide (Ag_2O) where 3 g of Ag_2O (*s*) was added to 3.5 L of nanopure water in a 5 L 3 neck Pyrex vessel. This mixture was heated to 70 °C and pressurized to 10 psi above atmosphere with H_2 gas.[22] The vessel was vented 4 times to ensure that a homogeneous hydrogen atmosphere was obtained. The colloids were successively filtered with 0.45 μm and 0.22 μm nylon filters. After filtering, the colloids were centrifuged at 150 g's for 8 hours at 4 °C to concentrate the particles for later use. Three final colloids were produced with dipole resonance maxima with optical densities (OD) at 427 nm (OD 19.5), 498 nm (OD 161.3), and 576 nm (OD 286.3) for colloids denoted A, B, and

C, respectively. The labels A-C are kept with the core particles as each subsequent reaction step is taken.

To estimate of the total surface area of silver in suspension, an aliquot of each suspension was removed and dissolved in 10 % nitric acid. The sample was then analyzed with ICP-OES to determine total silver concentration. Standards ranging from 100 ppb to 12 ppm were made using $AgNO_3$ dissolved in 10 % HNO_3. By using the diameter of silver particles and the total silver concentration an estimate of particle concentration was found that includes the total amount of silver in suspension, not just the silver in the spherical particles.

3.3.3. Synthesis of silica spacer

Ag:SiO_2 suspensions were prepared through a variation of the Stöber method by mixing 50 mL of 2-propanol and an amount of silver particle suspension. For each reaction the particle concentration was standardized such that each reaction mixture had the same total silver surface area. As such, 3.225 mL, 0.480 mL, and 0.688 mL of suspensions A-C, respectively, were diluted to 8 mL with nanopure water and added to the 50 mL isopropanol solution. To this suspension, 600μL of 30% ammonium hydroxide was added followed directly by the appropriate amount of tetramethoxysilane (TMOS): 0.75, 1.50, 3.00, and 5.00 μL for suspension 1-4 respectivly.[12] All liquids were kept in a cold room at 4 °C to obtain uniform temperatures before mixing, then sealed in an airtight container and left to react overnight. The particles were centrifuged and redispersed successively in 100% 2-propanol, 50% 2-propanol:water, and 100% water. After the last centrifugation, the particles were redispersed in 5 mL of water.

3.3.4. Synthesis of silver shell (completing CSS synthesis)

Core:spacer:shell (CSS) suspensions were prepared through a variation of the published method by Qian[27] and from modification of the hydrogen reduction method.[22] The Ag:SiO_2 particles were treated in tin (II) chloride ($SnCl_2$) then placed in a solution of Ag_2O (*aq*). The Sn^{2+} reduces Ag^+ (*aq*) to Ag^0 (*s*). As Ag metal is produced, it is hypothesized that it is electrostatically bound to the surface of the silica particle. The silver atoms on the surface of the particle are then considered to be anchors that will be the basis for the growth of highly crystalline islands that eventually coalesce into a silver shell.

3.3.4.1. Tin coating

In the first step, 12 mg of $SnCl_2$ were added to 30 mL of 0.013 M HCl solution and sonicated until completely dissolved. The appropriate volumes of the Ag:SiO_2 particles suspensions were added to the solution, 4 mL of A (OD 2), 2 mL of B (OD 8), 2 mL of C (OD 32), where the volume was varied such that the total surface area was again uniform for all suspensions. Once the suspension was added, the mixture was diluted to 40 mL so that the HCl concentration was 0.01 M.[27] The suspension was sonicated for 10 minutes, shaken for 1 hour, and centrifuged two times at 500 g's for 5 hours at 4 °C, redispersing in nanopure water each time.[27]

3.3.4.2. Silver seeding

The tin coated particles were cleaned via centrifugation, the whole suspension was quickly redispersed in a saturated silver oxide solution. The solution was prepared by placing 0.1 g of Ag_2O (*s*) in a 0.22 μm nylon filter and folding the filter paper such that the Ag_2O (*s*) is enclosed within the filter. The packet is suspended above the water

such that only the tip of the silver packet is submersed in water. This ensured that the Ag_2O (*s*) is never in direct contact with the particles. After 24 hours of exposure under gentle stirring, the suspensions were centrifuged for 5 hours at 500 g's at 4 °C. The suspension was redispersed in 7 mL of nanopure water.

3.3.4.3. Silver shell (H_2 reduction)

A saturated silver oxide solution was prepared in a quartz round bottom vessel by placing 0.3 g Ag_2O (*s*) in 250 mL of nanopure water under constant stirring. After stirring for 1 hour the appropriate aliquot of the silver-seeded suspension, typically 2 mL, was added such that the total surface area was held constant. The vessel was pressurized to 10 psi and vented 4-5 times so that a homogeneous hydrogen atmosphere existed above the mixture. The reaction was allowed to proceed for 3 hours before depressurizing the vessel and purging the reaction mixture with nitrogen gas to remove any dissolved hydrogen gas. The suspension, typically a dark brown color, is filtered with Fisherbrand® Quantitative Q5 filter paper. The filter paper was rinsed with 2 L of nanopure water before filtering the final suspension. Once filtered, the CSS particles were centrifuged at 500 g's for 5 hours at 4 °C. The particles were redispersed in 8 mL of saturated silver oxide solution.

In Figure 9, a graphical reaction scheme for the synthesis of the CSS particles, starting with a core particle synthesized by the H_2 reduction method, is shown. The scheme includes representative electron microscopy images of each of the steps with the silver color representing silver metal, blue-green representing the silica layer, and red representing Sn^{2+} ions. The CSS particle in the center of the Figure 9 is sectioned to show all layers.

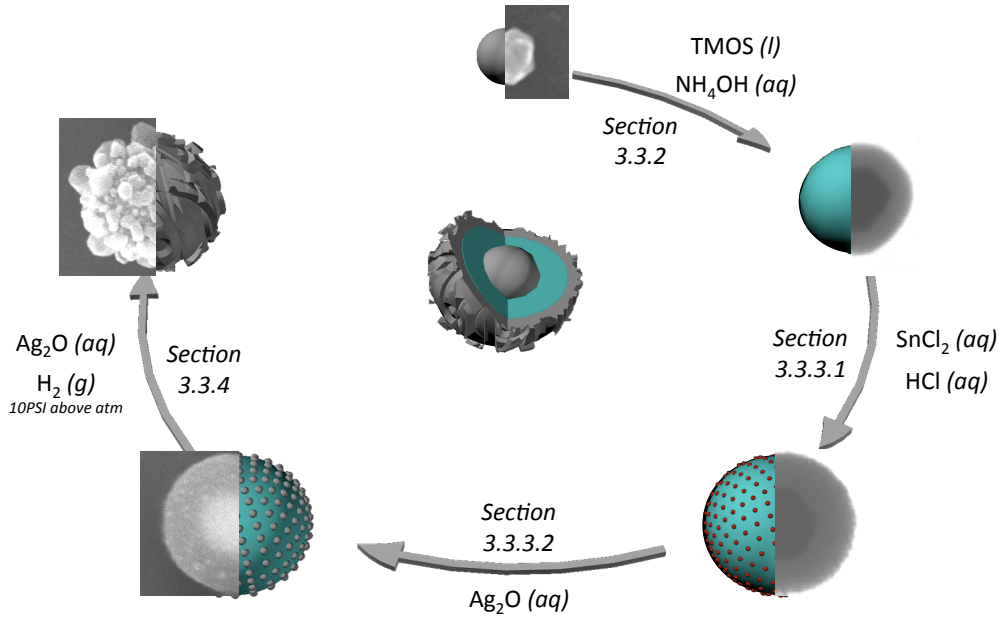

Figure 9. Schematic representation and STEM images of each step of the synthesis. Silver represents silver metal, blue-green represents silica, and red represents Sn^{2+}. The images are not from a consecutive set of particles and are scaled to fit the schematic.

3.4. EAS measurements

The absorption and scattering components of the extinction spectrum are separated through the use of an integrating sphere. The tungsten halogen lamp was energized and allowed to stabilize for 2 hours before collecting data. Lamp stability was confirmed by collecting multiple lamp spectra and ensuring acceptable overlap. The first step in the measurement was to obtain an extinction blank spectrum, taken with a 1 cm water-filled cuvette in the external sample holder and no cuvette in the integrating sphere. The second step was to obtain the absorption blank spectrum, captured with a 1 cm water-filled cuvette in the external sample holder and a 0.1 cm water-filled cuvette in the integrating sphere. The third step is to collect the extinction spectrum of an OD 1 suspension; this was done by adding 2 mL of the aforementioned suspension in the

external cuvette in the external sample holder with no cuvette in the integrating sphere. The last step is to collect the absorption spectrum, which was collected with a blank external cuvette and a 0.1 cm internal cuvette filled with 400 μL of the aforementioned suspension. The blanks were taken every fourth sample to ensure that the lamp spectrum was not changing. Between every sample the integrating sphere was opened for 20 seconds then closed and the temperature was allowed to equalize for 1 minute before taking a spectrum. The raw data was transformed into spectra using the program 'eas.m' executed with Octave (Appendix A.1).

3.5. Cross sections

The cross sections were estimated through back calculations of each dilution during the synthesis process. This method assumes that 100 % of the particles were collected during each step of the synthesis. Equation 7 is used to calculate the extinction cross section (σ_{exe}):

$$extinction = 0.434\sigma_{exe}bn \quad \textbf{(7)}$$

where the extinction is the value directly taken from an extinction spectrum, *b* is the pathlength in centimeters and *n* is the particle concentration in particles per milliliter. With the particle concentration estimations it is possible to calculate the efficiency of the particles, or how much light they interact with. For ease of comparison, EASeff are introduced as the ratio of EAS cross sections to the geometric cross sections. The EASeff were also calculated using the "eas.m" program whose code is given in Appendix A.

3.6. Raman/ SERS measurements

Before any data were collected, two spectral tests were preformed to characterize the alignment of the laser as well as characterize the beam width. In the first test, the

stage was set 150 μm beyond focus and scanned over the edge of a freshly cleaved silicon-wafer, taking measurements every 1μm over a 60 μm distance total, where the data was processed using the program "siedged.m" executed in octave (Appendix B.1). This plot of Intensity verses distance is characterized by a sigmoidal curve, which can be modeled with the function

$$I(x) = \frac{I_{max}}{2}\left[1 + \text{erf}\left(\frac{\sqrt{2}(x_0 - x)}{\omega_0}\right)\right] \quad \textbf{(8)}$$

where I(x) is the intensity profile, I_{max} is the max intensity of a particular band, x is the lateral distance from the cleaved edge of the silicon substrate x_0 and ω_0 is the beam waist. The error function erf(x) is used to model the sigmoidal curve and thus the ω_0 can be extracted from the fitted equation, which is calculated through minimization of the sum of the squares of the residuals.[37] Figure 10 shows a representative plot with the variables of the associated fit listed accordingly. These parameters allow one to calculate the scattering volume of the beam for both qualitative control and for quantitative measurements.

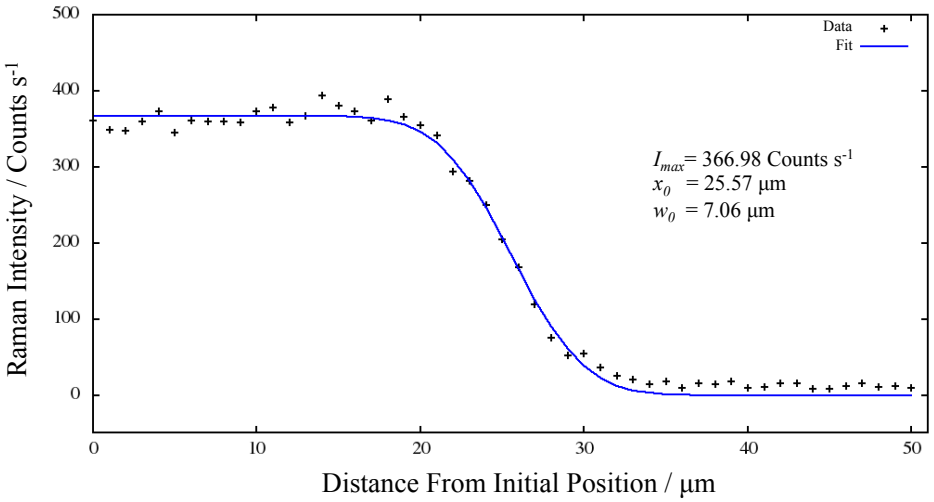

Figure 10. A plot of Raman intensity as the laser beam is scanned over a silicon wafer edge.

A second test was used to assess the confocality of the beam where focus was held on the silicon substrate and the aperture was gradually closed from 1000 μm to 0 μm taking measurements every 50 μm, where the data was processed using the program "siapeture.m" executed in octave (Appendix B.2). If the beam is centered there should a significant region where there is no change in the intensity of the silicon Raman signal.

Two aggregated SERS samples were prepared by mixing 3 mL of the Lee-Meisel colloid with 3 mL of a 53 mM KCl solution for 10 minutes. Taking 900 and 940 μL of the aggregated colloid and mixing with 100 and 60 μL of a 1 μM CV solution, the 100 and 60 nM SERS suspensions were prepared. The final mixtures were allowed to mix for an additional 5 minutes before measuring the SERS of the sample. SERS samples of the un-aggregated core samples, the 5 CSS samples, and the two SiO_2:Ag samples were prepared by mixing 900 and 950 μL of OD 1 colloid with 100 and 50 μL of the 1 μM CV solution, respectively. These samples were allowed to mix for 20 hours before measuring

the SERS signal. Additional measurements were taken after two weeks to assess the stability of the suspensions.

To measure the single molecule enhancement factor (SMEF), three stock solutions were made with crystal violet (CV, 1.0 mM), rhodamine 6G (R6G, 1.0 mM), and benzotriazole (BTA, 1.4 mM) dissolved in water. Each dye was measured with 3 second acquisitions and 50 averages with the beam focused on the surface of the liquid, followed directly by measuring the reference liquid, 2-bromo-2-methylpropane (BMP), neat with the same acquisition parameters. CV SERS samples were prepared by mixing 50 μL of a 1 μM CV solution with 950 μL of an OD 1 suspension of core, SiO_2:Ag, or CSS particles. The samples were allowed to mix for about 20 hours before being measured. The data was acquired over a 30 second period, taking a spectrum every 0.05 s.

The analytical enhancement factor (AEF), discussed in Section 4.4 (page 57) was also used to assess the usefulness of the particles as a SERS substrate. The 1 mM CV solution was measured with 3 s acquisition and 50 averages. The SERS samples were prepared as before and measured under the exact same conditions as the 1 mM CV solution. This data was fit, using the program Fityk, with a pseudo-Voigt function to extract peak areas and the error associated with the fits.[38]

CHAPTER 4. RESULTS & DISCUSSION

4.1. Synthesis

4.1.1. Core synthesis

Three sets of four (twelve total) CSS particles were synthesized for this work. The first step in the synthesis of CSS particles was to synthesize three different silver colloidal suspensions, denoted A, B, and C, in order of increasing size, to be used as the core particles. These colloids were created using the hydrogen reduction method (experimental details found in Section 3.3.2.2). The dipole resonance was monitored with UV-Vis until the desired dipole resonance maximum was obtained which was used to estimate particle size.[22] The colloids were filtered with a 0.45 μm and 0.22 μm nylon fiber membrane, which removed most of the silver rods and plates from the suspension.

Figure 11 shows the extinction spectra for each suspension with the dipole resonance labeled accordingly. The letter in the top left of the spectrum is the core particle label. The spectra show relatively narrow plasmon peaks with the tail at the long wavelengths falling down below the spectral minimum at 322 nm, which occurs due to the spectral overlap of the SPPR and interband transition. This gives some qualitative indication that there is no aggregation and that there is a narrow distribution of particles. The SEM images are paired with the spectrum directly above the image and the particle size distributions found from 100 measurements are listed below the image. The images are scaled to the same scale bar so the differences in particle size are reflected in the image.

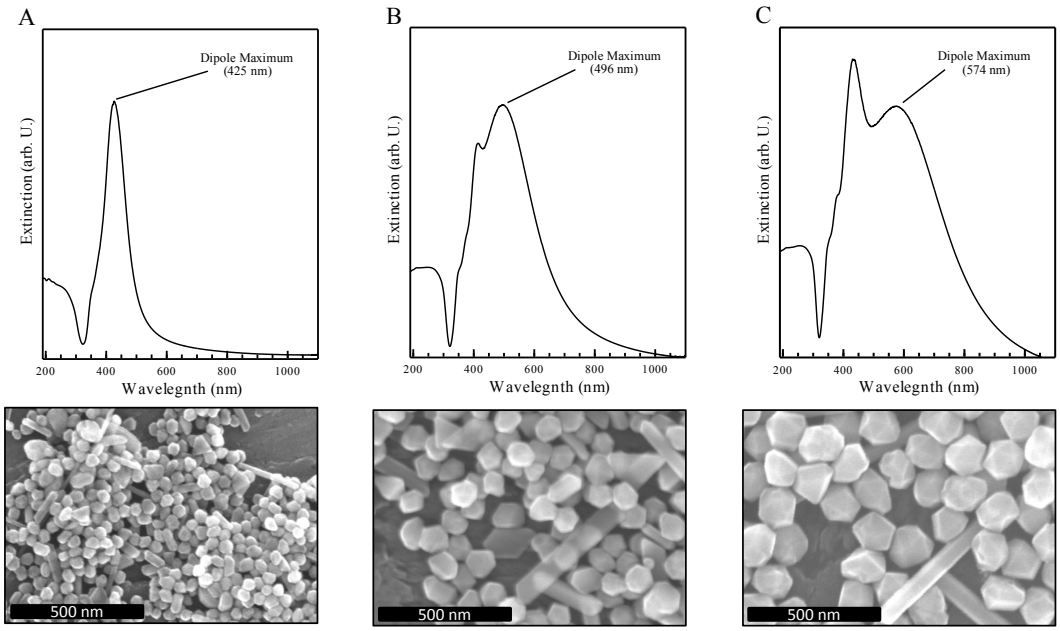

Figure 11. Extinction spectra of the colloidal particles that were used as the core particles with their associated SEM images. The images are set to the same scale.

SEM images for each suspension confirm that there is a small percentage of silver rods and plates, which is typical for the hydrogen reduction method. These morphologies are not accounted for in estimating the particle concentrations through published extinction cross sections for silver suspensions synthesized by the H_2 reduction method.[22] This becomes important when the total silver surface area is used to standardize each reaction in the next step of the synthesis. To account for the extra surface area, ICP-OES is used to find the total silver in suspension, and with the average diameter of the particles the number of particles is estimated. This assumes all particles have one diameter and that all particles are spherical. These assumptions are not completely accurate, but it was expected to be a better method for estimating total surface area of a reaction; especially when switching among different core particles. Figure 12 illustrates

the differences in surface area prediction when using the two estimation methods. It is seen that with the suspensions A and B the reference is an underestimate, and is an overestimate for the C suspension. While the underestimate of surface area seen for suspensions A and B were expected, the overestimate seen in C was not. The mean diameter of the particles in suspension C were larger than any reported in Reference 22 and as such the reference data was extrapolated to calculate an extinction cross section. The assumption of a linear trend in the reference data that was extrapolated may account for this overestimation.

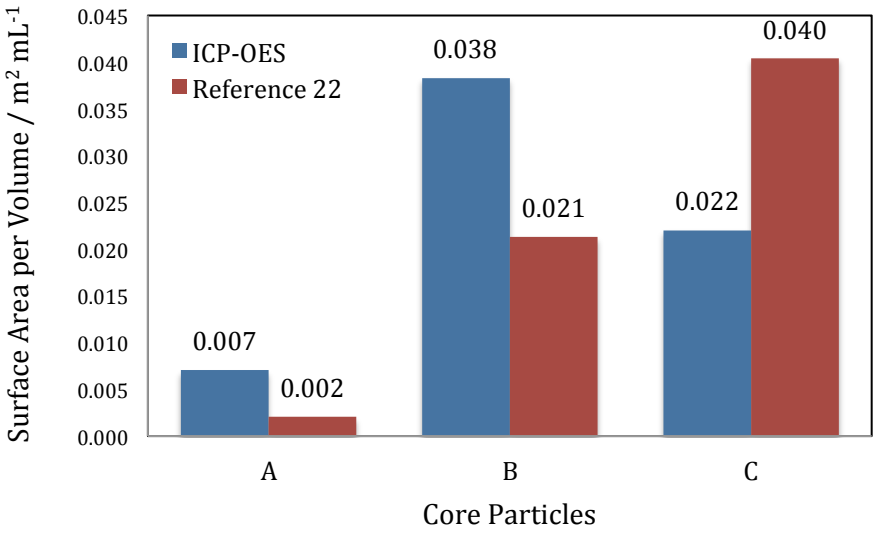

Figure 12. Estimation of total surface area per unit volume. The red and blue bars represent the surface area estimation using the reference manuscript[22] and ICP-OES standardized method.

4.1.2. Ag:SiO_2 Core-shell synthesis

To get similar silica spacers between the three core sizes the reaction mixture was proportioned such that each mixture had the same amount of 2-propanol, water and total surface area of silver. This method was developed in hopes that it would allow for

greater control in creating similar silica spacer thicknesses among the three core sizes. The synthesized Ag:SiO_2 particles were first analyzed with UV-Vis after they had been washed via centrifugation. The extinction spectrum for each of the 12 Ag:SiO_2 suspensions and the respective core suspensions are shown in Figure 13 with each core labeled at the top and with the silica thickness label (1-4) denoted in the plots. Below the plots are representative SEM/STEM images of the Ag:SiO_2 particles with the thinnest shell (1) at the top and the thickest shells (4) at the bottom of Figure 13 with the Ag:SiO_2 total diameter measurements below the images.

The silica shell causes a red shift in the plasmon resonance as silica displaces water as the local medium. Silica has a higher refractive index than water resulting in a reduction in the restoring force and thus a plasmon resonances that has shifted to longer wavelengths. Noting the change in dipole resonance before and after the silica spacer is added allows for some assessment of shell thickness. The change in the plasmon resonance is directly proportional to the shift in particle resonance for thin shells. However, as the spacer thickness becomes larger than the extension of the local EM field away from the particle surface during an SPPR, the particle can no longer "feel" changes to the local environment and exhibits the same resonance position for increasing thicknesses.[12]

Most of the images seen in Figure 13, with the exception of B1 and A4, were recently imaged, 7-8 months after their initial synthesis. Unfortunately, the images show a significant amount of particulate matter on the particle surface giving them a rough appearance. The samples were stored in plastic vials, which might have leeched plasticizers or binders into the suspension, that subsequently were included when the

samples were drop cast onto an indium tin oxide (ITO) slide. Furthermore, all 12 samples were drop cast onto the same ITO slide. Improper cleaning of the slide prior to drop-casting could also account for the contamination. The drop-cast samples were dried out in open air in the lab for one week before imaging. A spot plate covered the slide but some dust may have settled on the slide surface. Whatever the source of the contamination, it seems to have arisen in the past 6 months and not from the initial synthesis. This can be confirmed by the images of B1 and A4 (lower panels), which were taken soon after the synthesis and showed a smooth silica surface. These images are shown in Figure 13, where the lower image of B1 and A4 is that acquired previously, allowing for a quick comparison of the difference in the silica surfaces.

Total particle diameters and the associated standard deviation for each Ag:SiO_2 suspension were taken from at least 100 measurements of the particles. From comparing the images taken for suspension B1, the contamination issue seems to have had no effect on particle diameter. While total Ag:SiO_2 diameters are reported in Figure 13, the thicknesses of the silica layer are presented in Table 2 (page 49).

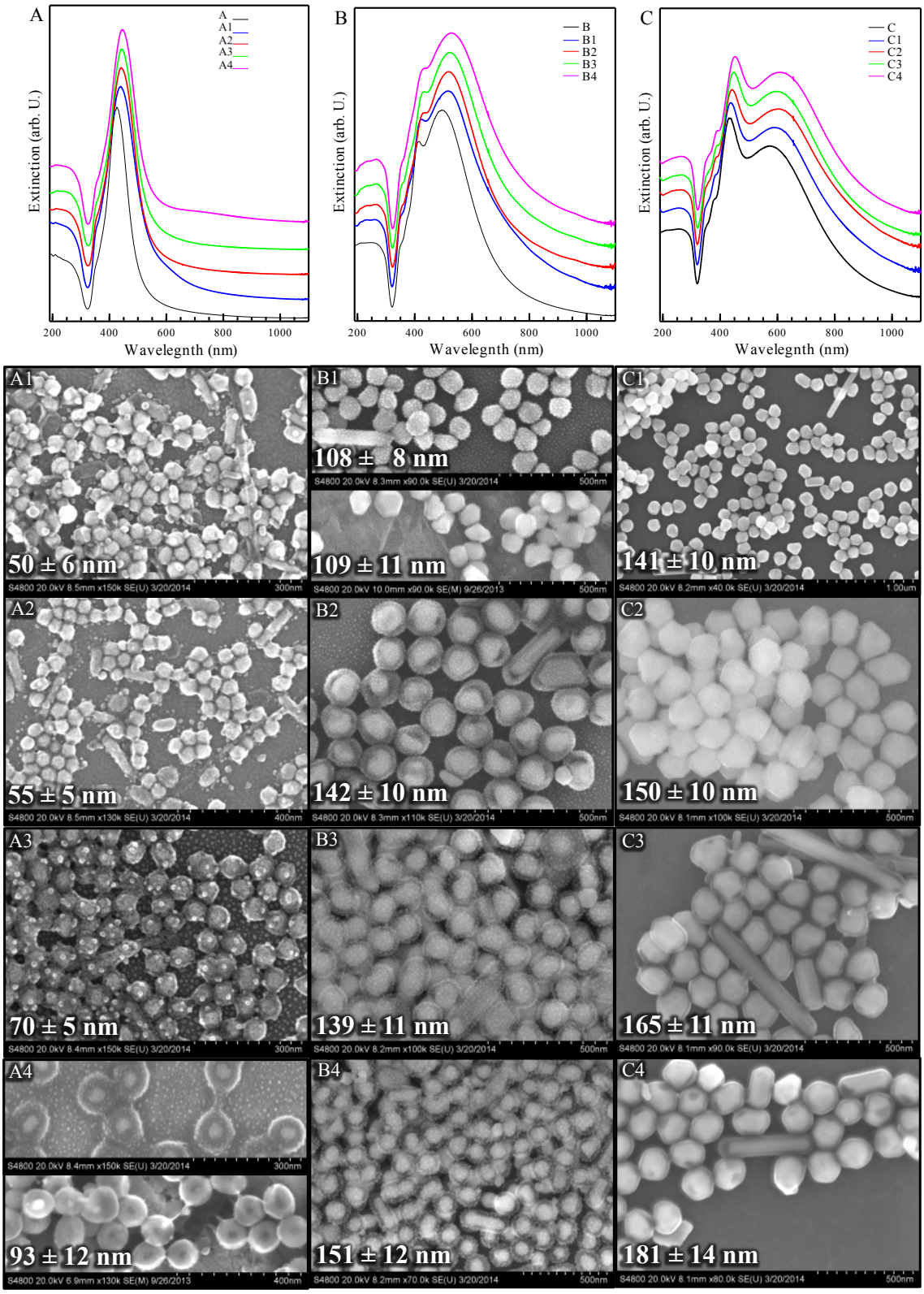

Figure 13. Extinction spectra of Ag:SiO_2 suspension with the associated SEM images.

4.1.3. Ag:SiO_2:Ag core:spacer:shell synthesis

Following silica coating, Sn^{2+} ions were added to the surface of the Ag:SiO_2 particles (Section 3.3.4.1) for the purpose of later reducing Ag^{+} (aq) to Ag^{0} (s) on the surface of the Ag:SiO_2 particles, which occurs spontaneously due to the reduction potential of Ag^{+} (*aq*) being 0.94 V higher than that of Sn^{2+} (aq). The Sn^{2+} ions are most likely bound to the electron rich silica though electrostatic interactions. This reaction is also monitored by UV-Vis where the Sn^{2+} seems to be further influencing the plasmon resonance resulting in another red-shift in the particle's extinction spectrum. The cause of this red-shift is not fully understood. The strong shift, regardless of the spacer layer thickness, would suggest that the Sn^{2+} ions penetrate into the porous silica layer.[19] This penetration could affect the SPPR in one of two ways. Most probably, the Sn^{2+} ions bind to both the exterior and interior of the silica layer, increasing the polarizability of the medium and thus reducing the core's restoring force. On the other hand, it is possible that the Sn^{2+} ions interact with silver oxide species on the surface of the core, reducing more silver and thus causing a plasmon shift due to a slightly increased size. Table 1 (page 42), lists the dipole SPPR position after each synthetic step prior to silver shell formation, illustrates the experimental shifts seen in this work.

Following Sn^{2+} treatment, the Ag:SiO_2 particles were exposed to a saturated silver oxide solution to initiate the silver decoration of the silica surface. In early trials of this procedure, it was found that silver oxide particulates would attach to the surface of the tin-treated Ag:SiO_2 particles during this exposure step. These particulates would later be reduced to silver metal leading to extremely asymmetric CSS particles. To ensure that Ag_2O (*s*) is not captured on the surface of the particle, the suspension is kept at room

temperature and the Ag_2O (*s*) is physically separated from the suspension via a folded nylon 0.1 μm membrane, in a manner that is similar to steeping a bag of tea. This helps to slow the reduction reaction so that the silver is gently attached to the surface. This suspension is centrifuged to concentrate the particles. The silver metal on the surface now serves as the anchor needed to initiate the growth of silver shells. This is also monitored with UV-Vis. Representative results are shown in Figure 14 where the black spectrum is the core particle, blue is $Ag:SiO_2$ suspension showing a 15 nm shift, red is tin coated particles showing a 18 nm shift from the original position, and green is the silver seeded particles which show a slight blue-shift back to 15 nm from the original position. Figure 14 also shows representative images of tin-treated $Ag:SiO_2$ particles before (red) and after (green) exposure to Ag_2O (*aq*). As can be seen in the image, small islands of silver metal are attached to the $Ag:SiO_2$ surface following Ag_2O (*aq*) exposure.

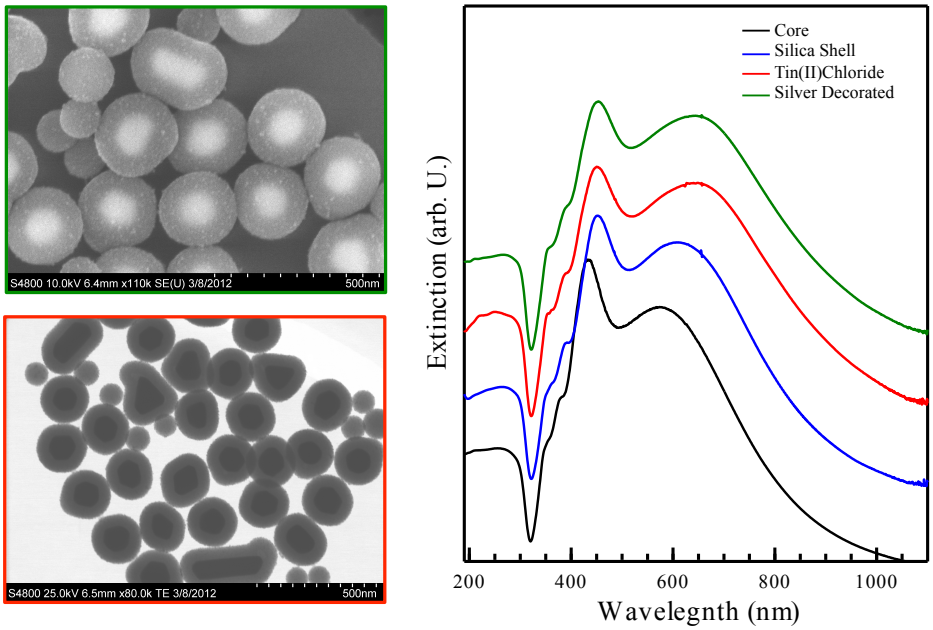

Figure 14. Representative shifts in extinction spectra for each step leading up to the silver shell synthesis. The plot shows the spectra for the original C colloid (black), the Ag:SiO_2 particle (blue), the Ag:SiO_2 -Sn^{2+} particle (red), and the Ag:SiO_2 seeded particle (green). The electron microscopy images are representative samples showing the Sn^{2+} treatment (red) and the Ag-decorated particles (green).

Table 1 shows dipole resonance position for suspensions in this work. For A suspensions the shifts were not as expected in that they displayed a further red shift in the dipole resonance position when the surface was seeded with silver. The unexpected shift in plasmon resonance is perhaps due to incomplete silica shells or to contamination during the synthesis steps. Suspensions B1 and B2 maintained the same extinction position during the silver seeding step, this is not understood and will be the subject of future studies. The remaining suspensions exhibited the expected blue-shifts in extinction spectra.

Table 1. Dipole resonance position for each step in the synthesis of CSS particles.

Sample	Core Dipole Position / nm	SiO_2 Dipole Position / nm	Sn^{2+} Dipole Position / nm	Ag^{0} Dipole Position / nm
A1	427	439	439	441
A2		443	436	438
A3		444	440	443
A4		446	441	445
B1	496	516	518	518
B2		519	530	531
B3		524	545	528
B4		528	559	527
C1	576	592	632	630
C2		603	638	636
C3		600	654	650
C4		609	645	641

The final step in synthesizing the CSS particles was to grow a silver shell around the silver-seeded Ag:SiO_2 particles. 2 mL of the silver-treated Ag:SiO_2 suspensions were placed in a 3-necked quartz vessel. Quartz, which is pure silicon dioxide and does not readily induce the formation of independent silver nanoparticles,[22] was employed so that any newly reduced silver accumulates on the surface of the Ag:SiO_2 particles. As the seeded surface collects silver, the seeds on the surface grow into highly crystalline domains of silver. As these domains of silver get larger they eventually coalesce into a silver shell. The result of the reaction is a rough raspberry-like shell. The spectra and SEM/STEM images of the associated CSS suspensions are shown in Figure 15. The spectra labeled A-C (left to right) with the SEM/STEM images of each CSS particle

starting with the thinnest silica spacer on top moving to the thickest silica spacer at the bottom of the Figure 15. For suspensions in which CSS particles were successfully synthesized, the particle diameter and size distributions listed within the images.

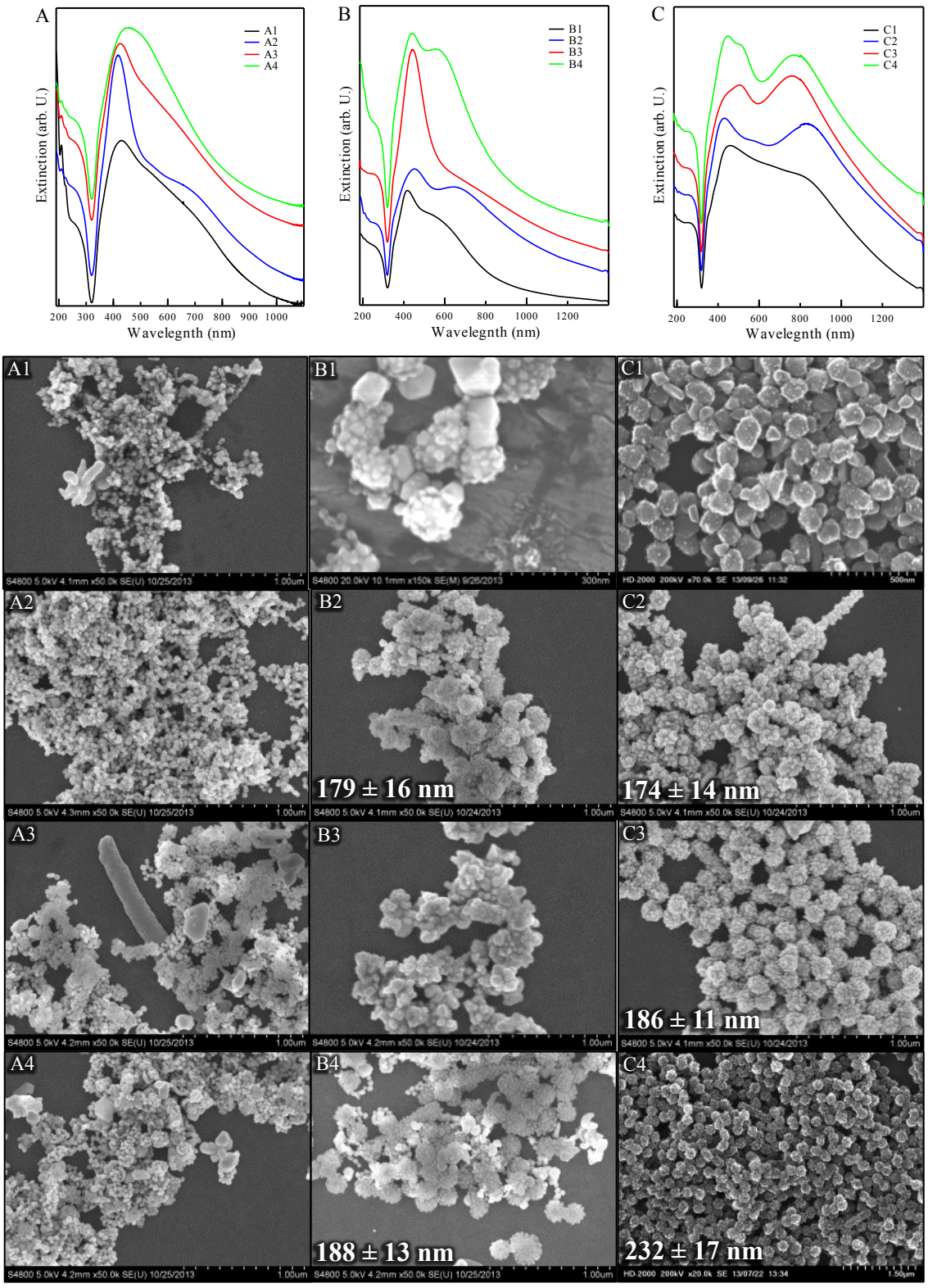

Figure 15. Extinction spectra of CSS suspensions with the associated SEM images.

Visual inspection of the SEM images of the CSS suspensions prepared in this work (Figure 15) clearly shows that some of the reactions did not create shells as planned. The silica spacer layer denoted with a 1 (top row in Figure 15), which was synthesized with 0.75 μL of TMOS, only appears to have made a complete shell in the case of the B cores. However, at least some silica must have coated all 3 of the silver core suspensions as the suspensions could be centrifuged at high speed without agglomeration, which is not possible with bare silver suspensions, and the particles do not appear to be significantly etched from interaction with NH_4OH (*aq*). In each case for the "1" spacer layers, independent silver particles are present suggesting that few silver seed anchors were available on the $Ag:SiO_2$ surface for growth. In the case of B1, the $Ag:SiO_2$ particles appear to contain a complete shell with typically at least 1 larger silver particle attached to the silica surface. This scenario may indicate that the B1 particle surface was approaching a minimum number of silver seeds needed to form the complete raspberry surface seen in other CSS images. A useful future study would be to both determine the minimum concentration of TMOS needed to form a complete silica shell and to determine how silver seed density on the $Ag:SiO_2$ surface is related to silica thickness.

The rest of the "A" suspensions were quite heterogeneous with many independent silver nanoparticles mixed with the CSS particles (Figure 15 A2-4). Although some suspensions do appear to contain complete shells, most notably A4, there are also a significant number of free particles in suspension, which may be the result of the smaller surface area of the "A" $Ag:SiO_2$ particles. The smaller surface area might not support the same sized islands of silver as a larger particle, and as the islands get too large they

detach from the Ag:SiO_2 particle and grow in the suspension independently. In all CSS synthesis conducted in this study, the hydrogen reduction reaction for shell growth was allowed to proceed for 3 hours. Given that the particle concentrations were made such that each reaction mixture contained the same total surface area on which to grow shells, it was expected that the shells would grow to the same thickness. A useful future study would be to determine the relationship between Ag:SiO_2 diameter and appropriate silver shell synthesis reaction times and thus the silver shell thickness that can be produced.

The final incongruity among the images presented in Figure 15 is that of the B3 particles, in which the image shows large aggregates of particles that are much to large to be the proposed CSS particles. This is likely the result of contamination in the reaction vessel as it appears that the silver-seeded Ag:SiO_2 particles coalesced with large masses of silver growing on top of the agglomerates.

Moving forward with the study, only the CSS suspensions C4, C3, C2, B4, and B2 seemed sufficiently complete and uniform to warrant further analysis. These particles have a uniform appearance with a minimal amount of independent silver particles. Although some of the other synthesized suspensions contained CSS particles, a suitable method to separate the CSS particles from the independent silver particles was not available. As such, further spectral analysis of the suspension would not represent the true physical behavior of the CSS particles contained within that suspension. A summary of the particle sizes is shown below in Table 2 where the diameter of the core is shown with the thicknesses of each additional layer.

4.1.4. SiO_2:Ag core:shell synthesis

SiO_2:Ag particles were synthesized to assess what effect the core particle has on the silver shell. These particles were intended to have the same final diameter as some as the C4 suspension so that a comparison of the plasmon resonances of the shell with and without the silver core could be made. Figure 16 show the extinction spectra for both shell suspensions synthesized denoted D and E. The SEM images show raspberry-like shells with a minimal amount of independent silver particles. Suspension D has a diameter that is comparable to the C4 suspension. As such, these two suspensions will be compared extensively in subsequent sections.

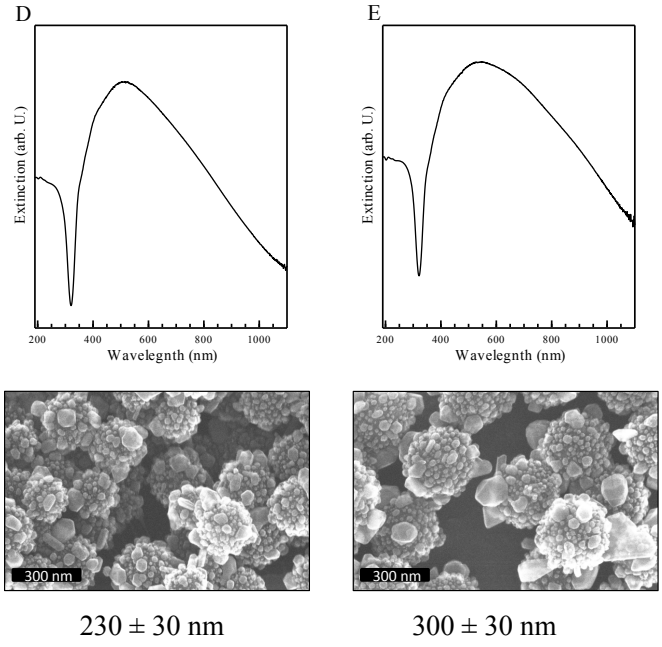

Figure 16. Extinction spectra for SiO_2:Ag particles D and E, with the STEM images of each shown below along with average particle sizes and size distributions.

4.1.5. Particle dimensions summary

A summary of the particle sizes is shown below in Table 2 where the diameter of the core is shown with the thicknesses of each additional layer. The silica thicknesses

were determined by subtracting the core diameter from the Ag:SiO_2 diameter and dividing by 2. The same procedure was used to derive the silver shell thickness, however this assumes that the silica shell is not changing during the steps following the Ag:SiO_2 reaction. As can be seen in the table, varying the TMOS amount among reaction mixtures with normalized silver surface area typically provided reasonable control over layer thickness. The cause of the lack of control of specific reactions (B2 and B3) is not understood and should be the subject of future study.

Table 2. Particle sizes and uncertainties. The core measurements are shown as the diameter. The spacer and shell measurement are shown as the thickness as applied to the surface of the core particle and spacer, respectively.

Suspension	(material) Core / nm	(silica) Spacer Thickness / nm	(silver) Shell Thickness[a] / nm	Total Diameter[a] / nm
A1	(silver) 51 ± 4	< 1	-	-
A2		2.5 ± 3	-	-
A3		10 ± 3	-	-
A4		21 ± 3	-	-
B1	(silver) 103 ± 8	2.5 ± 3	-	-
B2		20 ± 6	19 ± 11	179 ± 16
B3		18 ± 7	-	-
B4		24 ± 7	19 ± 10	188 ± 13
C1	(silver) 141 ± 8	< 1	-	-
C2		4 ± 7	12 ± 7	174 ± 14
C3		12 ± 8	11 ± 8	186 ± 11
C4		20 ± 9	26 ± 11	232 ± 17
D	(silica) 164 ± 28		33 ± 5	230 ± 30
E	(silica) 230 ± 29		35 ± 5	300 ± 30

[a](-) Denotes a value that could not be extracted due to the failed synthesis of the silver shell.

4.2. Theoretical Spectra for CSS particles

A common method for assessing synthesized suspensions is by comparing measured extinction spectra to those calculated through Mie's solutions for Maxwell's equations.[13] This is an involved calculation and beyond the scope of this research so an online program was utilized to model layered plasmonic particles.[39] In modeling these CSS particles, the silver and silica are modeled as perfectly crystalline and spherical with

the diameters of the particles in suspension all being exactly the same. These results are shown in Figure 17, with the extinction spectra for the complete CSS particles in black and the theoretical spectra shown in blue. In Figure 17 the plots are labeled using the naming convention described in Figure 7. The calculations show some very sharp resonances in each extinction spectrum. One cause of the sharp resonances, is likely due to strong light extinction originating from Fano resonances.[36,40] These resonances occur due to interference between resonant scattering occurring simultaneously at multiple surfaces leading to an asymmetry between the absorption and scattering modes of the extinction spectrum.[41] The Fano resonance in each calculated spectrum is the longest wavelength spike (denoted with an asterisk in Figure 17), which seems to overlap with the much broader dipole resonance. As will be discussed in Section 4.3, the CSS articles synthesized in this study are far more absorptive than is expected from calculation, likely due to the additional absorption pathways resulting from the rough features on the shell. The additional absorptive nature of the CSS particles likely lowers the probability of a Fano resonance, which is due to resonant scattering. As can be seen in the panel labeled "Core C" in Figure 17, the calculation also tends to show far sharper multipole resonances, even for the core particles. Higher order resonances tend to be more sensitive to crystalline defects such that even with the highly crystalline hydrogen reduction method particles, the experimental efficiency of the quadrupole and octupole resonance are significantly lower than expected. Of course, spectral differences are also expected when considering that the CSS shell morphology is quite rough when compared to the perfectly smooth shells of the calculations.

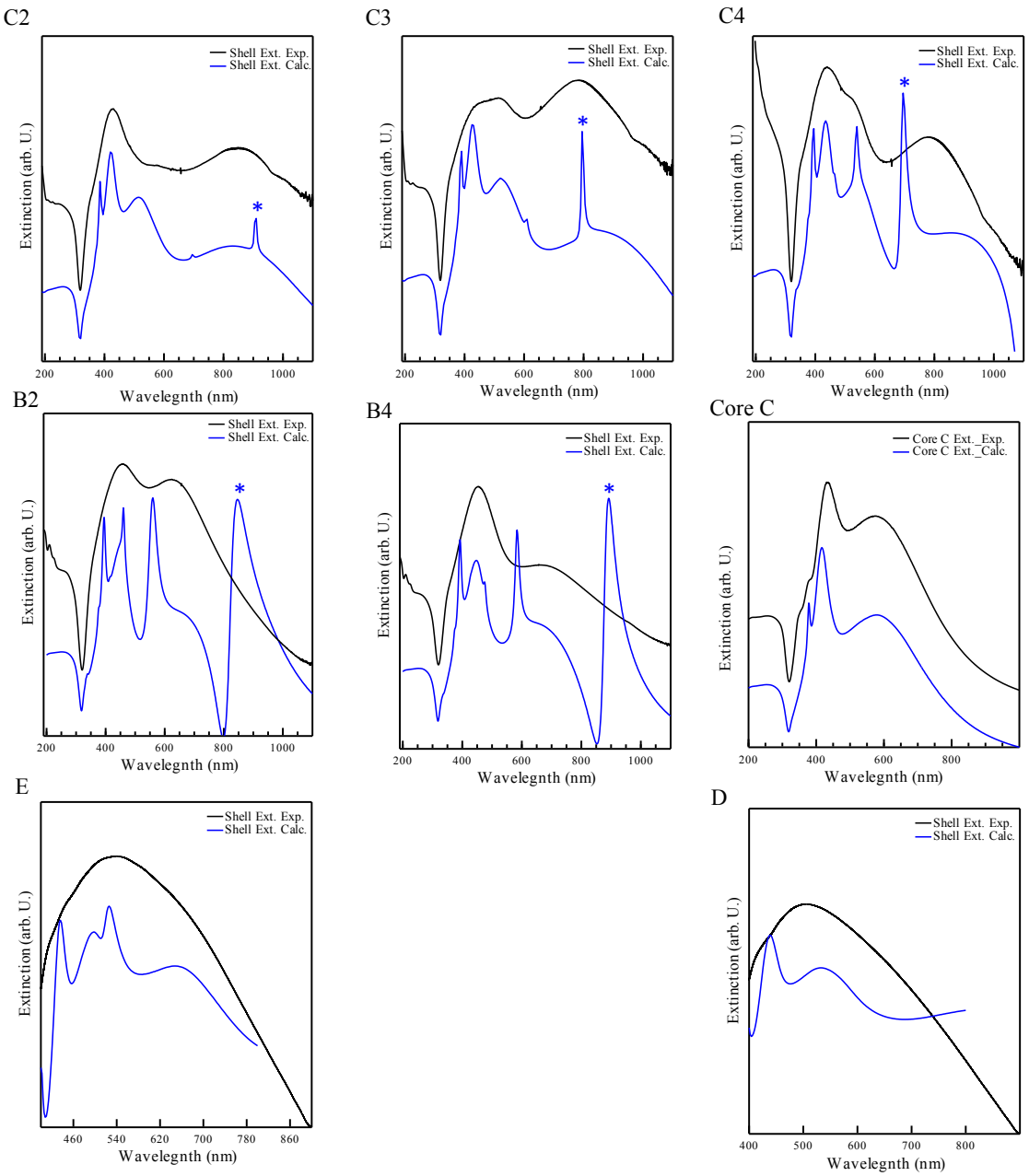

Figure 17. Theoretical spectra (blue) and actual spectra (black) for CSS particles. (*) Denotes Fano resonances.

Despite the differences in the morphology of the shells, a similar overall spectrum is seen in which the broad shape of the spectra overlay well for most of the suspensions. To gain further insight into the evolution of CSS extinction spectra with increasing shell

thickness, an additional CSS suspension was grown using C3 Ag:SiO_2 particles. Aliquots were taken every 30 minutes over a 3 hour reaction time (Figure 18). The theoretical spectra are shown, in order to model the growth of the shell as time progressed. The first spectrum, at the bottom of Figure 18, shows both the theoretical and the actual extinction for the core particles. The next spectrum shows the extinction for an Ag:SiO_2 particle. The third spectrum (A) shows a CSS particle with a 5 nm shell and each additional spectrum assumes an increase in shell thickness of 5 nm. The third spectrum (B) is a spectrum taken of the suspension after 30 minutes of reduction with each additional spectrum representing the suspension after an additional 30 minutes. When the results are stacked on the same plot it is evident that, though the particles are different from the assumptions made by the theoretical calculations, the model still exhibits the similar shifts in resonance as silver shell increases in size.

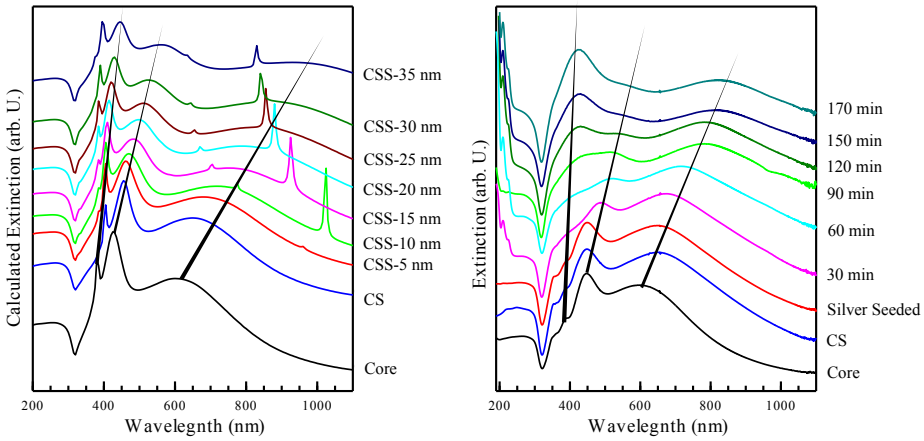

Figure 18. Growth study of CSS particle synthesis for calculated (left) and experimental (right) spectra.

4.3. EAS, cross sections, efficiencies

To gain a more thorough understanding of the relaxation pathways of the CSS particles, it is necessary to deconvolute the scattering and absorption components from the extinction spectrum. To do this, an integrating sphere was used to quantify the true absorption of the suspension. By subtracting the absorption spectrum from an extinction spectrum taken with the same instrumentation, the scattering component of the SPPR relaxation can be calculated (cf. Figure 6).

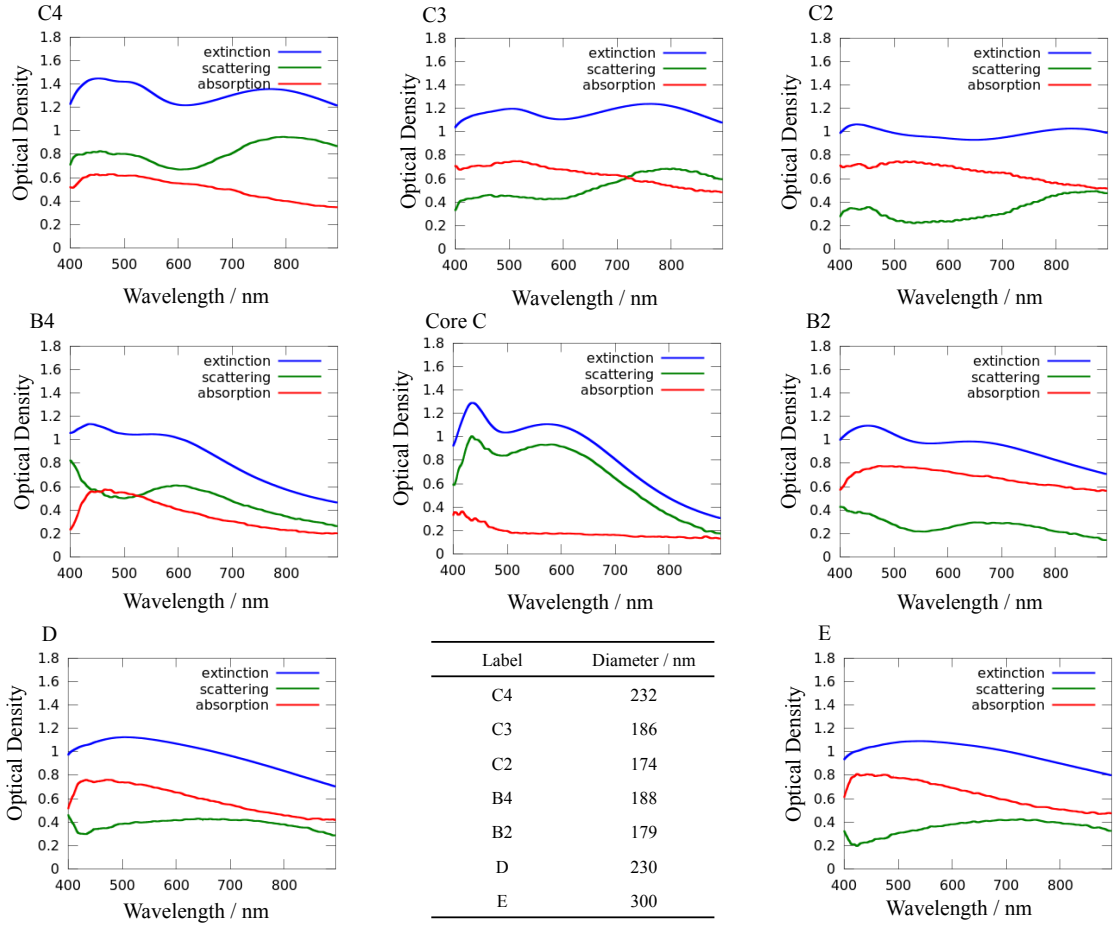

Label	Diameter / nm
C4	232
C3	186
C2	174
B4	188
B2	179
D	230
E	300

Figure 19. EAS spectra for CSS and SiO_2:Ag particles. The extinction (blue) is the sum of the scattering (green) and the absorption (red) components.

The spectra in Figure 19 reveal some interesting trends. Firstly, when comparing the actual C4 (CSS) spectrum to the calculated spectra (cf. Figure 20), it is observed that CSS particles are more highly absorptive than predicted. This is likely due to the rough features that make up the silver shell in which the collective oscillation of the shell is responsible for the resonant scattering and the resonances supported in the individual particles that make up the shell cause absorption. Likewise, stark differences are seen when comparing the spectra of the C4 (CSS) particles and those of the D (SiO_2:Ag) particles. These two suspensions have very similar overall diameters and similar silver shell thicknesses. It is particularly interesting to note the significant red-shift in the dipole extinction maximum of the CSS particles as compared to that of the SiO_2:Ag particles. When considering that the summation of the extinction spectra of the D shells and the C cores could not produce such a red-shifted dipole maximum, it would seem that the plasmon modes of the core are coupling with that of the shell in the CSS particles.

Further potential evidence of coupling can be seen when comparing C2 and C3 CSS particles and B2 and B4 CSS particles. As can be seen in Table 2, for each set of CSS particles both the core and shell sizes are constant with changes occurring only in the spacer thickness. From Figure 19, it is clear that a thinner spacer leads to both a red-shifted dipole extinction maximum and an increase in the absorptive nature, relative to the total extinction, of the resonance. SPPR coupling provides stabilization to the system, increasing the time of electron oscillation. Because resonant scattering is the faster relaxation pathway, increasing oscillation time increases the probability of the absorption relaxation pathway.[11]

EAS cross sections, which are a measure of the light extinguished by a single particle, were also calculated for the CSS particles using Equation 7. Particle concentrations were estimated using the procedure outlined in Section 3.5. This procedure assumes that there are no losses between synthesis steps, This assumption is most likely not accurate as the centrifugation steps typically experience some losses, such that the reported extinction cross sections are an underestimate of the actual cross sections.

In Figure 20, the wavelength-dependent efficiencies of CSS extinction, scattering, and absorption are shown, as well as the predicted efficiencies of the C4 CSS suspension, which is representative of all the CSS suspensions. Table 3 shows the measured efficiency values at λ = 450 nm. The data reveals that the CSS particles of the C series are significantly more efficient than that of the B series. An interesting comparison is that of the C2 and B2 CSS suspensions and that of the C3 and B4 suspensions. In each of the two cases, the overall particle diameters are quite similar (cf. Figure 19, Diameter Table), however the C series particles are nearly twice as efficient as the B series. This is a somewhat surprising result when considering that the C core efficiencies are actually less than that of the B cores.[14]

When comparing the C4 CSS spectrum to the calculated spectrum, it can be seen that the actual extinction efficiency is ca. twice what is predicted, with the vast majority of the additional extinction being caused by absorptive SPPR relaxation. The fact that the increase in absorption efficiency seems to occur over all wavelengths suggests that the reason the rough shell of the CSS particles extinguishes light similarly to the calculated behavior. Examination of the electron microscopy images in Figure 15 reveals

that the silver shells are not fully percolated, suggesting that the individual particles that make up the shell have a coupled dipole resonance. Dipole coupling causes a significant red-shift of the plasmon mode, and that coupling causes an increase in absorptive relaxation.[28] In the case of the CSS particles, the absorption component of the extinction is influenced by both the small shell particles acting independently (absorption at ca. 400 nm) and as a coupled shell structure (absorption at longest wavelength extinction maximum). The addition of these absorptions has a broad impact on the overall absorption profile measured in the study presented in Figure 20.

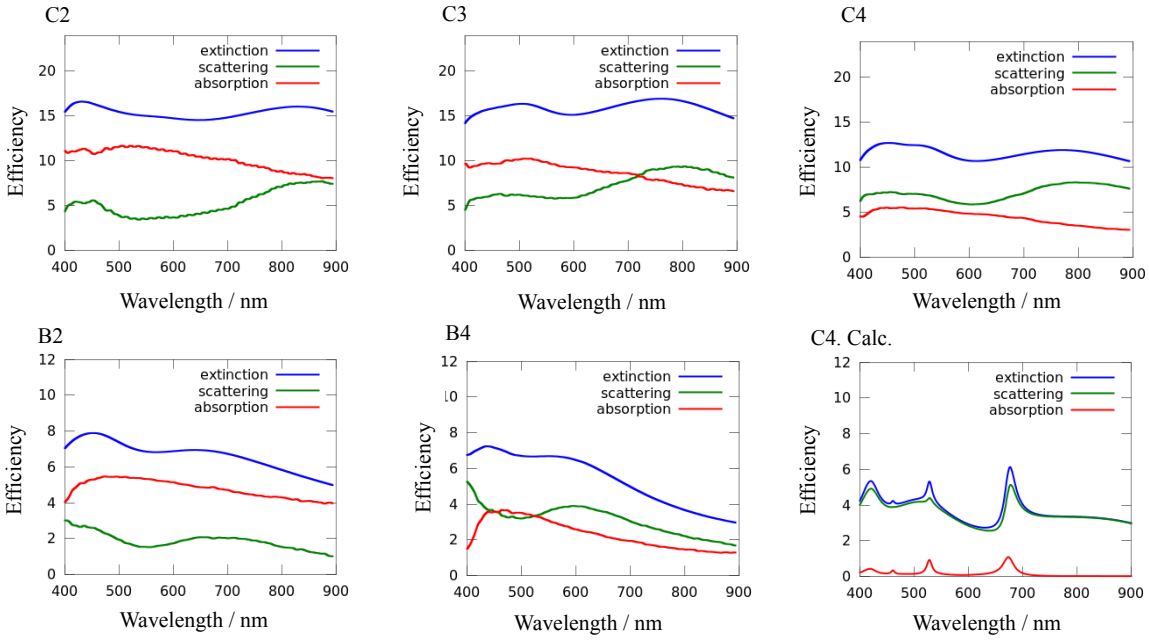

Figure 20. EAS efficiencies of the 5 CSS suspensions and C4 calculated spectrum.

Table 3. EAS efficiency values at a wavelength of 450 nm.

Label (diameter)	Extinction Efficiency at λ = 450 nm	Scattering Efficiency at λ = 450 nm	Absorption Efficiency at λ = 450 nm
C4 (232 nm)	12.7	7.2	5.5
C3 (186 nm)	15.8	6.1	9.6
C2 (174 nm)	16.4	5.6	10.8
B4 (188 nm)	6.8	3.3	3.5
B2 (179 nm)	7.9	2.6	5.3

There were several attempts to more quantitatively estimate CSS particle concentration and thus efficiency. The preferred method for obtaining these measurements is known as standard subtraction.[14] In the case of the silver shell particles synthesized by the method described in this document however, the standard subtraction method negatively impacted CSS morphology, as particles seemed to be too fragile to extract them from a suspension. This process begins with an indium tin oxide (ITO) coated glass slide coated with poly(4-vinylpyridine) (PVP). The coated glass slide is placed in a suspension of particles with a precisely known dipole plasmon extinction maximum near OD 1 and gently agitated for several hours. During this time particles are adsorbed to the polymer due to the interaction of the particles with the lone pair of electrons on the nitrogen in the pyridine. When the slide is removed from the suspension, the extinction of the suspension is measured, and the difference in extinction is indicative of the number of particles that were removed. By counting the particles on the slide it is possible to estimate the number of particles removed from the suspension and calculate the extinction cross section via Equation 7.[14]

When this process was employed with shelled particles, the extinction spectrum of the suspension changed following exposure to the PVP-coated slide. Subsequent electron microscopy of the exposed ITO slides revealed small particles of silver on the slide with sparse amounts of shell particles that had partially fallen apart (Figure 21). This indicates that the electrostatic attraction that holds the silver shell to the silica surface is relatively weak. Several attempts were made to gently remove the particles by not agitating the slides during exposure or by lowering the temperature of the suspension during PVP-slide exposure. Unfortunately these attempts were not successful and the aforementioned dilution method was employed to estimate particle concentrations.

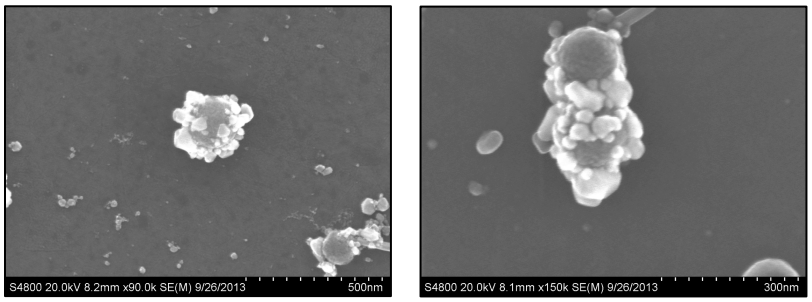

Figure 21. SEM images of slides used in standard subtraction of silver shells on a silica core.

4.4. Raman enhancement factor

The single molecule enhancement factor (SMEF) method outlined by Le Ru et al, which was used to characterize single molecule SERS among aggregated Lee-Meisel particles, utilized a LabRam Raman instrument with a 100x water immersion objective with a N.A. of 1.0.[37] Optically, this is much different from the 10x dry objective used for this study, however the results were comparable to each other and with a few modifications to the method and sample preparation it could be a valuable technique for this lab. In the SMEF method a standard reference molecule is employed to calculate the cross sections of a chosen dye molecule. The reference chosen was BMP using the area under the 516 cm^{-1} band and an absolute differential cross section $(d\sigma_{RS}/d\Omega)_{ref} = 5.4 \times 10^{-30}$ cm^2 sr^{-1}. To calculate the differential cross section of dye molecules the following formula is used:

$$\left(\frac{d\sigma_{RS}}{d\Omega}\right)_{samp} = \left(\frac{d\sigma_{RS}}{d\Omega}\right)_{ref} \cdot \left(\frac{I_{samp}}{I_{ref}}\right) \cdot \left(\frac{C_{ref}}{C_{samp}}\right) \quad \textbf{(9)}$$

is used where $(d\sigma_{RS}/d\Omega)_{samp}$ is the differential cross section of the sample, I_{samp} is the area under a particular band of the dye spectrum (CV, 804 cm^{-1} and 918 cm^{-1}), I_{ref} is the area under the 516 cm^{-1} band of the reference spectrum, C_{samp} is the molar concentration of the dye solution (1 mM dissolved in water), and C_{ref} is the molar concentration of the reference measured neat (8.76 M).[37] Using the program "SMEF.m" the code for which is given in Appendix B, the time resolved Raman spectra were processed and plotted as the SMEF over time. This should illustrate how the SERS analyte signal changes over time as particles move in and out of focus via Brownian motion. Figure 22 shows data acquired on this instrument and displays a relatively constant signal. This is believed to be a result of the low N.A. 10x objective employed for this study where the increase in

sampled volume is allowing for many silver particles/aggregates to move in and out of focus creating a constant Raman signal. If the optics are correctly aligned and the SERS systems are optimized there should be spikes in the enhancement factor that correspond to large SERS signal resulting from molecules on particle hot spots and lulls that correspond to no SERS signal. Due to the constant SMEF, it is not possible to determine the number of particles that are being probed in any given acquisition. Perhaps changing to a higher N.A. 10x objective with a longer acquisition time or using a lower concentration of silver particles would allow for the signal change needed to calculate the SMEF on this particular instrument.

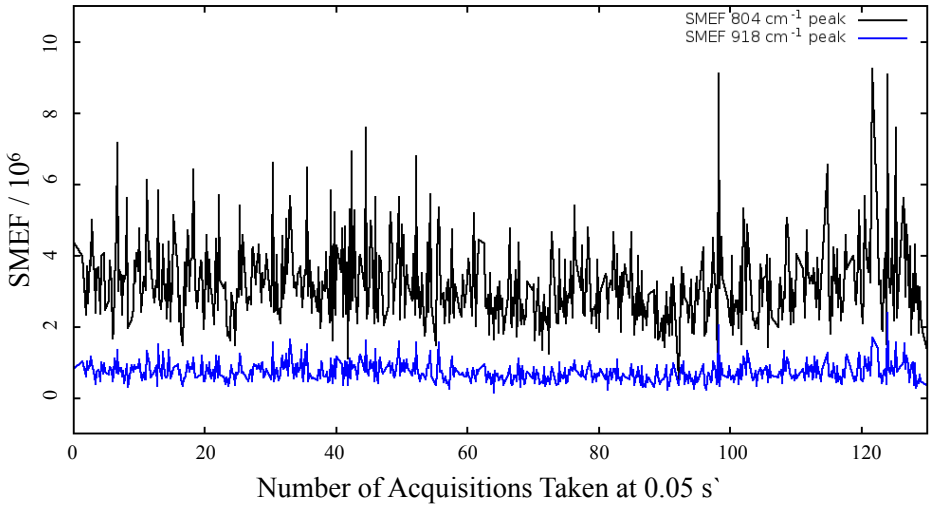

Figure 22. A plot of the SMEF over time for an aggregated Lee-Meisel colloid with 10 nM CV calculated using both the 804 and 918 cm^{-1} Raman bands.

Due to time constraints, the SMEF method was not pursued further and the analytical enhancement factor (AEF) method was then employed to calculate the enhancement factors. This method uses average intensities of the SERS samples whereas the SMEF method characterizes the signal from a single molecule. A 1 mM solution of

CV was always measured immediately before any SERS samples. The peak areas of bands 804 and 918 cm^{-1} were calculated by the program Fityk as previously mentioned (Section 3.6) and the areas were extracted such that they could be used in the calculation of the AEF. The AEF was calculated from the equation:

$$\mathrm{AEF} = \frac{I_{SERS}/C_{SERS}}{I_{samp}/C_{samp}} \quad \textbf{(10)}$$

where I is the area under a particular Raman band and C is the concentration of the analyte in that particular measurement, and the subscript *SERS* indicates the SERS sample while the subscript *samp* is the non-SERS measurement.[37] The raw spectra are shown in Figure 23 A, where the non-SERS measurement is multiplied by 4 and subtracted by 40,000 so that the two spectra are on a comparable scale. Plots B and C in Figure 23 show the baseline fitted spectra, from 780 to 970 cm^{-1} with pseudo-Voigt function peaks in green and the sum of the fits shown in red with the residuals plotted below the fitted data. Gaussian and Lorentzian functions were also used to fit the data, however the pseudo-Voigt function, which is a combination of Gaussian and Lorentzian functions, fit the Raman bands much more efficiently in terms of minimization of the residuals, as is typical in Raman spectroscopy, and was therefore chosen.

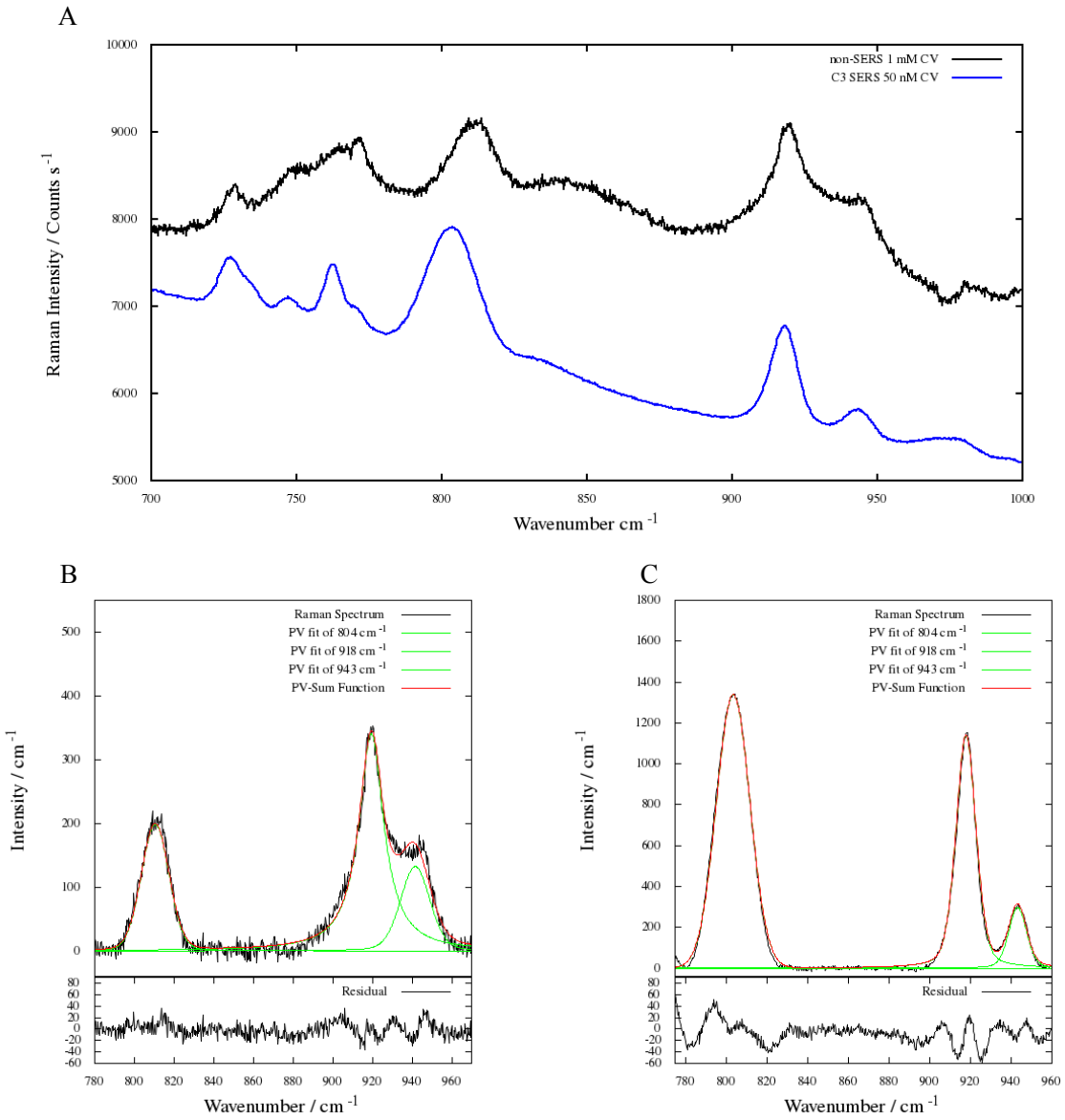

Figure 23. Representative Raman spectra with no corrections (A), and baseline corrected and fitted spectra of 1 mM CV non-SERS (B) and 50 nM CV SERS with unaggregated C3 CSS particles (C).

The remaining fitted data is shown in Appendix C with the AEF results shown in Table 4. The uncertainties for peak area were reported with the Fityk fit parameters such that the uncertainty in the AEF was calculated from error propagated through Equation 10.

When comparing the data presented in Table 4, it is clear that the classic Lee-Meisel (L-M) aggregation method provided the largest level of SERS enhancement. This is not surprising when considering that the action of aggregation occurs after the analyte has been added to the suspension and is likely to trap analyte molecules between particles, ensuring a high level of enhancement. All CSS particles also presented reasonable SERS enhancement, with the C3 and C4 CSS suspensions presenting enhancements within one order of magnitude of the to the L-M aggregation method. When comparing the CSS enhancement to the L-M enhancement, it is important to note that the CSS enhancement occurs *without* aggregated particles.

To better gauge the enhancement factor of the CSS particles, SERS measurements were attempted under the same measurement conditions with un-aggregated B and C core particles and D SiO_2:Ag particles. In the case of the B and C core particles, no SERS signal was detected. Likewise, little SERS signal was seen for the D SiO_2:Ag particles. Given that the outer surface of the B, C, D, and CSS particles are all silver synthesized by the same method and all particles are suspended in saturated silver oxide solution, it is reasonable to assume that the CV molecules approach and perhaps adsorb to the particles' surface with equivalent efficiency. As such, the data suggest that the local EM field surrounding the CSS particles is either much stronger or extends much farther than either the core or SiO_2:Ag particles. Alternative explanations to consider are that the CSS particles simply have a greater surface area and thus are more likely to adsorb/interact with CV or that the relatively weakly bound particles of the silver shell detach and aggregate around CV molecules. A comparison of the enhancement factors of D and C4 however, would seem to nullify those explanations, given that the overall diameters,

surface morphologies, and shell synthetic protocols of the particles are identical. Instead, the data suggests that the much larger enhancement of the CSS particles is caused by the interaction of the silver core and silver shell through plasmon coupling allowing for substantial enhancement without the need for aggregation.

Another trend found in the data of Table 4 is that the enhancement factor of a 50 nM CV solution is higher than that of a 100 nM solution. This is likely due to the fact that this marginal increase in concentration does not appreciably affect the number of CV molecules that make close approach and/or adsorb to the silver surface. This is most likely due to the dye molecules slow approach to the surface of the silver particles; as such the higher concentration of dye particles is not high enough to affect the adsorption process. A useful future study would be to quantify the relationship between analyte concentration and SERS enhancement factor.

Table 4. Peak areas and AEF values with associated uncertainties.

Colloid[a]	Concentration CV / nM	AEF[b] (804 cm^{-1})	Percent Uncertainty[b]	AEF[b] (918 cm^{-1})	Percent Uncertainty[b]
L-M*	60	1.39×10^6	3.03	9.12×10^5	3.17
L-M*	100	1.44×10^5	2.87	8.95×10^4	3.05
B4	50	1.34×10^4	3.09	1.09×10^4	3.82
B4	100	1.65×10^3	3.00	1.30×10^3	3.20
B2	50	2.89×10^4	3.03	2.21×10^4	3.42
B2	100	2.40×10^3	2.88	1.92×10^3	3.17
C4	50	2.19×10^5	2.95	1.31×10^5	3.04
C4	100	1.53×10^4	2.99	1.26×10^4	3.04
C3	50	7.57×10^5	3.14	4.62×10^5	3.23
C3	100	7.04×10^4	3.09	4.12×10^4	3.37
C2	50	7.53×10^3	3.57	8.10×10^3	4.22
C2	100	1.02×10^3	2.96	8.16×10^2	3.09
D^+	50	-	-	-	-
D^+	100	7.28×10^1	-	3.80×10^1	-
E^+	100	-	-	-	-
B & C#	50	-	-	-	-
B & C#	100	-	-	-	-

[a](*) Denotes classic Lee-Meisel aggregation, (+) denotes SiO_2:Ag core:shell particles, and (#) denotes un-aggregated core suspensions. [b](-) Is in place of a value that could not be extracted from the associated spectrum due to weak/no Raman signal.

CHAPTER 5. CONCLUSION & FUTURE DIRECTIONS

The synthesis of Ag:SiO_2:Ag CSS particles via the hydrogen reduction of Ag_2O (s) is a successful and repeatable method, though there is less control in the final shell morphologies than was previously anticipated. The CSS surface exhibits a raspberry-like appearance consisting of highly crystalline domains of silver that collectively behave similarly to a continuous, smooth silver shell. The silver domains seem to be weakly bound to the surface of the silica spacer surface. Future studies should include developing alternative methods of decorating the silica surface with silver to create more robust particles.

As the silica spacer is reduced in size the particle's true absorbance is increased, suggesting electromagnetic coupling between the core and the shell that allows the particle to dissipate energy non-radiatively. Also, electromagnetic coupling of the individual silver domains in the shell layer is contributing to the increased absorption efficiency. The increased coupling is leading to an efficiency that this almost twice what was predicted. Conversely, as silica spacer thickness increases, coupling is apparently reduced and scattering becomes the larger component of the extinction spectrum most likely originating from the core particles' plasmon resonance.

Unaggregated CSS particles, although not performing quite as well as aggregating Lee-Meisel particles, exhibited substantial SERS enhancement factors. When comparing the enhancement factors of the CSS particles to those of either core or shell particles, it would seem that the enhancement is caused by the coupling of the core and shell.

Overall the synthesis protocol developed in this project produces particles of the desired configuration. However, there are substantially more questions that need to be answered to completely develop a reliable protocol to synthesize robust CSS particles with predictable dimensions. A future study that might be of interest would be to functionalize the silica layer with molecules such as APTMS or PVP and adsorb various-sized silver colloids to the surface in a series of reactions to see if the spherical array of particles will act as a shell. This could provide a way to systematically model and measure the plasmonic properties of these particles in a more timely fashion. If one could coat a core particle in hydrogel, a gel that swells/contracts with variation in solvent polarity, then attach silver particles to the outer surface of the gel, the resulting CSS particle might provide a more systematic approach to study core-shell coupling in a CSS particle.

It would likewise be of interest to adsorb silver seeds to an APTMS-modified silica spacer layer followed by silver shell growth via the hydrogen reduction method. If the particles on the surface are strongly held in place, then perhaps a more thorough measurement of the EAS cross sections and efficiencies could be completed.

CHAPTER 6. WORKS CITED

(1) Jain, P. K.; Huang, X.; El-Sayed, I. H.; El-Sayed, M. A. *Acc. Chem. Res.* **2008**, *41*, 1578.

(2) Kim, S.-S.; Na, S.-I.; Jo, J.; Kim, D.-Y.; Nah, Y.-C. *Appl. Phys. Lett.* **2008**, *93*, 073307.

(3) Kneipp, K.; Kneipp, H. *Acc. Chem. Res.* **2006**, *39*, 443.

(4) Li, J. F.; Huang, Y. F.; Ding, Y.; Yang, Z. L.; Li, S. B.; Zhou, X. S.; Fan, F. R.; Zhang, W.; Zhou, Z. Y.; Wu, D. Y.; Ren, B.; Wang, Z. L.; Tian, Z. Q. *Nature* **2010**, *464*, 392.

(5) Zhang, J. Z. *J. Phys. Chem. Lett.* **2010**, *1*, 686.

(6) Halas, N. J.; Lal, S.; Chang, W.-S.; Link, S.; Nordlander, P. *Chem. Rev.* **2011**, *111*, 3913.

(7) Kneipp, K.; Kneipp, H.; Itzkan, I.; Dasari, R. R.; Feld, M. S. *Chem. Rev.* **1999**, *99*, 2957.

(8) Premasiri, W. R.; Moir, D. T.; Klempner, M. S.; Krieger, N.; Jones, G.; Ziegler, L. D. *J. Phys. Chem. B* **2005**, *109*, 312.

(9) Dong, J.; Qu, S.; Zhang, Z.; Liu, M.; Liu, G.; Yan, X.; Zheng, H. *J. Appl. Phys.* **2012**, *111*, 093101.

(10) Mirsaleh-kohan, N.; Iberi, V.; Simmons, P. D.; Bigelow, N. W.; Vaschillo, A.; Rowland, M. M.; Best, M. D.; Pennycook, S. J.; Masiello, D. J.; Guiton, B. S.; Camden, J. P. *J. Phys. Chem. C* **2012**, *3*, 2303.

(11) Evanoff, D. D.; Chumanov, G. *Chemphyschem* **2005**, *6*, 1221.

(12) Evanoff, D. D.; White, R. L.; Chumanov, G. *J. Phys. Chem. B* **2004**, *108*, 1522.

(13) Mie, G. *Ann. der Physic* **1908**, *25*, 337.

(14) Evanoff, D. D.; Chumanov, G. *J. Phys. Chem. B* **2004**, *108*, 13957.

(15) Johnson, P. B.; Christy, R. W. *Phys. Rev. B* **1972**, *6*, 4370.

(16) Sun, Y.; Xia, Y. *Science* **2002**, *298*, 2176.

(17) Brito-Silva, A. M.; Sobral-Filho, R. G.; Barbosa-Silva, R.; de Araújo, C. B.; Galembeck, A.; Brolo, A. G. *Langmuir* **2013**, *29*, 4366.

(18) Stöber, W.; Fink, A. *J. Colloid Interface Sci.* **1968**, *26*, 62.

(19) Wright, J. D.; Sommerdijk, N. A. J. M. *Introduction in Sol-Gel Materials Chemistry and Applications*; Philips, D.; O'Brian, P.; Robert, S., Eds.; Vol. 4.; CRC Press: Washington, D.C., 2001; pp. 1–14.

(20) Lee, C.; Meisel, D. *J. Phys. Chem.* **1982**, *86*, 3391.

(21) Creighton, J. A. *J. Chem. Soc., Faraday Trans. 2* **1979**, *75*, 790.

(22) Evanoff, D. D.; Chumanov, G. *J. Phys. Chem. B* **2004**, *108*, 13948.

(23) Biedermann, G.; Sillen, L. G. *Acta. Chem. Scand.* **1960**, *14*, 717.

(24) Danscher, G. *Histochemistry* **1981**, *71*, 1.

(25) Jackson, J. B.; Halas, N. J. *J. Phys. Chem. B* **2001**, *105*, 2743.

(26) Burry, R. W.; Vandré, D. D.; Hayes, D. M. *J Histochem. Cytochem.* **1992**, *40*, 1849.

(27) Zhu, M.; Qian, G.; Hong, Z.; Wang, Z.; Fan, X.; Wang, M. *J. Phys. Chem. Solids* **2005**, *66*, 748.

(28) Malynych, S.; Chumanov, G. *J. Am. Chem. Soc.* **2003**, *125*, 2896.
(29) Sio, A.; Shell, C.; Plasmon, N. D.; Shanthil, M.; Thomas, R.; Swathi, R. S.; Thomas, K. G. *J. Phys. Chem. Lett.* **2012**, *3*, 1459.
(30) Jablonski, A. *Nature* **1933**, *131*, 893.
(31) Fleischmann, M. H. P. J. and A. J. M. *Chem. Phys. Lett.* **1974**, *26*, 163.
(32) Qin, L.; Zou, S.; Xue, C.; Atkinson, A.; Schatz, G. C.; Mirkin, C. A. *PNAS* **2006**, *103*, 13300.
(33) Zhang, J.; Gryczynski, I.; Gryczynski, Z.; Lakowicz, J. R. *J. Phys. Chem. B* **2006**, *110*, 8986.
(34) Bardhan, R.; Mukherjee, S.; Mirin, N. A.; Levit, S. D.; Nordlander, P.; Halas, N. J. *J. Phys. Chem. C* **2010**, *114*, 7378.
(35) Hu, Y.; Noelck, S. J.; Drezek, R. A. *ACS Nano* **2010**, *4*, 1521.
(36) Ho, J. F.; Luk'yanchuk, B.; Zhang, J. B. *Appl. Phys. A* **2012**, *107*, 133.
(37) Le Ru, E. C.; Blackie, E.; Meyer, M.; Etchegoin, P. G. *J. Phys. Chem. C* **2007**, *111*, 13794.
(38) Wojdyr, M. *J. Appl. Crystallogr.* **2010**, *43*, 1126.
(39) Juluri, B. K.; Huang, J.; Jensen, L. Extinction, Scattering and Absorption efficiencies of single and multilayer nanoparticles https://nanohub.org/resources/nmie.
(40) Mukherjee, S.; Sobhani, H.; Lassiter, J. B.; Bardhan, R.; Nordlander, P.; Halas, N. J. *Nano Lett.* **2010**, *10*, 2694.
(41) Luk'yanchuk, B.; Zheludev, N. I.; Maier, S. a; Halas, N. J.; Nordlander, P.; Giessen, H.; Chong, C. T. *Nat. Mater.* **2010**, *9*, 707.

APPENDIX A. EAS PROGRAM

A.1 EAS program to be executed with Octave/MATLAB.

eas.m

```
%date created 13-10-21 by James P. Cook
%date modified 14-3-8 by JPC
clf
clear
% This program will take Extinction and Absorption intensities, transform them into Abs
spectrum, Calculate the scattering spectrum, display EAS cross section spectra, EAS
efficiencies, and display the three spectra on a graph. It creates 3 figures total if you
have the particle dimensions and particle concentration (particles per mL).  To execute
this program the Zenity package must be installed, available at
<http://octave.sourceforge.net/zenity/>

%%%%%%%%%%%%%%%%%%%%%%%%%%%%%%%%%%%%%%%%%%%%%%%%%%%
%----------------Begin user input------------------
%%%%%%%%%%%%%%%%%%%%%%%%%%%%%%%%%%%%%%%%%%%%%%%%%%%

choice = menu('Have you created a folder to store your figures? {Press Ctrl+C to
cancel}','Yes','No');

%%%%%%%%%%%%%% select/make directory %%%%%%%%%%%%%%
switch choice
  case{1};
     disp('Next, select the folder where the figure will be dumped.{Press enter when
ready}')
     pause
     fighome = zenity_file_selection([],'directory');

  case{2};
     disp('Create a folder to store the figures. Name the folder after your sample.
Please do not include spaces in the folder name, numbers and underscores are
acceptable');
return

end
lw       = 2;
ftype    = '-dpng';
fres     = '-r100';
fileout1 = [fighome '/figure1.png'];                % Name of figure
fileout2 = [fighome '/figure2.png'];                % Name of figure
fileout3 = [fighome '/figure3.png'];                % Name of figure

%%%%%%%%%%%%%%%%%%% select files %%%%%%%%%%%%%%%%%%%

disp('select your extinction blank spectrum. {Press enter when ready}')
pause
eb = load (zenity_file_selection);                  % extinction blank 'Io'
disp('select your absorbption blank spectrum. {Press enter when ready}')
pause
e  = load (zenity_file_selection);                  % extinction 'I'
disp('select your absorption spectrum. {Press enter when ready}')
pause
ab = load (zenity_file_selection);                  % absorption blank 'Io'
disp('select your extinction spectrum. {Press enter when ready}')
pause
a  = load (zenity_file_selection);                  % absorption 'I'

%%%%%%%%%%%%%%%%%%%%%%%%%%%%%%%%%%%%%%%%%%%%%%%%%%%%
```

```
%----------------End user input---------------------
%%%%%%%%%%%%%%%%%%%%%%%%%%%%%%%%%%%%%%%%%%%%%%%%%%

%========== Transform into Abs Spectra =============
x  = eb(:,1);
eb = eb(:,2);
ab = ab(:,2);
e  = e(:,2);
a  = a(:,2);

ext = -1*log10(e./eb);%-log(I/Io)=abs
abs = -1*log10(a./ab);%-log(I/Io)=abs

%===== Start data smoothing (Savitzky Golay) =======
gapsize = 1001;
  gp    = gapsize - 1;
  wd    = (gp)/2;
  tmp   = 1:wd;
  pk    = tmp(wd)+1;
  gap   = [tmp pk fliplr(tmp)];

  i     = gap/sum(gap);                              % area of gap(triangle) = 1

extsm       = conv(ext,i);
npts        = length(extsm);
extsm([1:gp (npts-gp+1):npts])=[];

absmooth    = conv(abs,i);
npts        = length(absmooth);
absmooth([1:gp (npts-gp+1):npts])=[];

xorg = x;
npts = length(x);
x([1:wd (npts-wd+1):npts])=[];

absmooth1 = absmooth;
extsm1    = extsm;

%=============== Scattering Calc ==================
absm1 = absmooth1.*30;
scat1 = extsm1 - absm1;

%-------------------------------------------------
%%%%%%%%%%%%%%%%%% Start Plot 1 %%%%%%%%%%%%%%%%%%
%-------------------------------------------------

% extsm %
subplot(2,2,1)
hold on
plot(xorg,ext,'linewidth',2)
plot(x,extsm,'linewidth',2,'color',[1 0 0]);
hold off
legend('extsm','ext')
xlabel('Wavelegnth / nm')
ylabel('Extinction')
axis tight

% absm %
subplot(2,2,2)
hold on
plot(xorg,abs,'linewidth',2)
plot(x,absmooth,'linewidth',2,'color',[1 0 0]);
hold off
legend('absm','abs')
xlabel('Wavelegnth / nm')
ylabel('Extinction')
axis tight
```

```
% EAS %
subplot(2,2,3)
plot(x,[extsm1 absm1 scat1],'linewidth',2)
legend('extinction','absorption','scattering')
xlabel('Wavelegnth / nm')
ylabel('Extinction');
axis tight;


print(fres,ftype,fileout1);

%-------------------------------------------------
%%%%%%%%%%%%%%%%%%%%%%%%%%%%%%%%%%%%%%%%%%%%%%%%
%-------------------------------------------------

choice = menu('Do you know the particle diameter and concentration','Yes','No')

switch choice
  %--------- calc EAS Xsect & eff spec ----------%
  case{1};
    value = 1;

    D = input('What is the particle diameter in nanometers')
    D = D*10^-7;
    r = D/2;
   Ar = pi*(r)^2;

    clf
    n = input('What is the particle concentration particles/mL')

  %----- This loop calculates EAS Xsect & eff ------%
    [npts,scrap] = size(extsm);
    for i = [1:npts];
        extXsect(i,:) = extsm1(i,:) / (0.434*1*n);
          exteff(i,:) = (extXsect(i,:)/Ar);

        absXsect(i,:) = absm1 (i,:) / (0.434*1*n);
          abseff(i,:) = (absXsect(i,:)/Ar);

        sctXsect(i,:) = scat1 (i,:) / (0.434*1*n);
          scteff(i,:) = (sctXsect(i,:)/Ar);
    end

  %%%%%%%%%%%%%%%%%%%%%%%%%%%%%%%%%%%%%%%%%%%%%%%%
  %-------------- plot figure 2 ---------------------%
  %%%%%%%%%%%%%%%%%%%%%%%%%%%%%%%%%%%%%%%%%%%%%%%%

  clf
  % Xsect %
  subplot(2,1,1)
  plot(x,[extXsect,absXsect,sctXsect],'linewidth',2)
  legend('extinction','absorption','scattering')
  xlabel('Wavelegnth / nm')
  ylabel('EAS cross section')
  axis tight

  % eff %
  subplot(2,1,2)
  plot(x,[exteff,abseff,scteff],'linewidth',2)
  legend('extinction','absorption','scattering')
  xlabel('Wavelegnth / nm')
  ylabel('EAS efficientcy');
  axis tight;

  print(fres,ftype,fileout2);

  %%%%%%%%%%%%%%%%%%%%%%%%%%%%%%%%%%%%%%%%%%%%%%%%
  %-------------- plot figure 3 ---------------------%
```

```
  %%%%%%%%%%%%%%%%%%%%%%%%%%%%%%%%%%%%%%%%%%%%%%%%%%%%%%%%%%%%%%%%

  % EAS graph %
  clf
  plot(x,[extsm1 absm1 scat1],'linewidth',2)
  legend('extinction','absorption','scattering')
  xlabel('Wavelegnth / nm')
  ylabel('Extinction');
  axis([400 800 0 2]);

  print(fres,ftype,fileout3);
  return

  %%%%%%%%%%%%%%%%%%%%%%%%%%%%%%%%%%%%%%%%%%%%%%%%%%%%%%%%%%%%%%%%
  %------------------ End of Path ------------------
  %%%%%%%%%%%%%%%%%%%%%%%%%%%%%%%%%%%%%%%%%%%%%%%%%%%%%%%%%%%%%%%%


%-------------------------------------------------%
 case{2}

  %%%%%%%%%%%%%%%%%%%%%%%%%%%%%%%%%%%%%%%%%%%%%%%%%%%%%%%%%%%%%%%%
  %------------- Plot EAS figure 2 -----------------
  %%%%%%%%%%%%%%%%%%%%%%%%%%%%%%%%%%%%%%%%%%%%%%%%%%%%%%%%%%%%%%%%

  % EAS graph %
  clf
  plot(x,[extsm1 absm1 scat1],'linewidth',2)
  legend('extinction','absorption','scattering')
  xlabel('Wavelegnth / nm')
  ylabel('Extinction');
  axis([400 800 0 2]);

  print(fres,ftype,fileout2);

  %%%%%%%%%%%%%%%%%%%%%%%%%%%%%%%%%%%%%%%%%%%%%%%%%%%%%%%%%%%%%%%%
  %-------------------------------------------------
  %%%%%%%%%%%%%%%%%%%%%%%%%%%%%%%%%%%%%%%%%%%%%%%%%%%%%%%%%%%%%%%%

end
```

Script ends here.

APPENDIX B. RAMAN PROGRAMS

B.1 Scan Over Edge Test to be executed with Octave/MATLAB.

siedge.m

```
clear
% Po = (pi*Wo^2)*Io/2
% Po = laser power at sample = 7.41mW

all = load ('SOE150.txt'); % 150 microns beyond focus
org = all;
[nspec,npts] = size(org);
x = org(1,2:npts);
dist= org(2:nspec,1);
org(:,1) = [];% cropping the data such that
org(1,:) = [];% only the specta are in the matrix
[nspec,npts] = size(org);
y = org;
x = 1:npts;

      [nspec,npts] = size(y);
                cx = [6 73 151 192 267 296 439 600 682 784 873 1000];
              [junk,slect] = size(cx);    % (1x13)
                 for i = 1:slect;
                        cy(i,:) = cx(:,i)-5:cx(:,i)+5;
                 end

for i = 1:nspec;
              spec = y(i,:);
                [npts,junk] = size(cy);
                       for j = 1:npts;
                            specy(1,j) = mean(spec(cy(j,:)));
                        end
                 p = polyfit(x(cx),specy,4);
               fit = polyval(p,x);
        Y(i,:) = spec - fit;
end

clear spec
      [nspec,npts] = size(Y);
for i = 1:nspec;
    spec(i,:) = max(Y(i,500:550));% pulls out the max values
end

scatter(dist,spec);
save('ascii','spec');
return
```

Code ends here.

B.2 Aperture Test to be executed with Octave/MATLAB.

siaperture.m

```
clear
% Po = (pi*Wo^2)*Io/2
% Po = laser power at sample = 7.41mW
% Io = intensity at focal plane =
% Po = 7.41
all = load ('Apet.txt');
org = all;
[nspec,npts] = size(org);
x = org(1,2:npts);
dist= org(2:nspec,1);
org(:,1) = [];% cropping the data such that
org(1,:) = [];% only the specta are in the matrix
[nspec,npts] = size(org);
y = org;
x = 1:npts;
clear spec
      [nspec,npts] = size(y);
for i = 1:nspec;
    spec(i,:) = max(y(i,450:600));% pulls out the max values
end
maximum = max(spec);
for i = 1:nspec;
    spec(i,:) = spec(i,:)/maximum*100;% pulls out the max values
end
scatter(dist,spec);
xlabel('hole / microns')
ylabel('percent intensity')
return
```

Code ends here.

B.3 Single molecule enhancement factor calculation to be executed with Octave/MATLAB.

EF.m

```
clear
lw       = 3;  % linewidth
fres     = '-r300';
ftype    = '-dpng';
fs       = 30; % fontsize
fighome  = '~/Octave/james/EF-2014-2-25/';
fileout = [fighome 'S3EF.png'];

                      % ----------- notes ----------- %
%%%%%%%%%%%%%
% Take CV dye spectra centered at 850 cm-1
% Integrate bands at 808 and 917 cm-1
% Take 2B2MPropane centered at 520 cm-1
% integrate band at 514 cm-1
% 1800 groove mm-1 grating
% acquisition time 0.05
% no averages.  aquired over 1 minutes time
%%%%%%%%%%%%%
                       % ------ Important!!! ------- %
% its important to center the grating at the above stated position, this ensures that the
peak positions will be in the correct place.
% change the fileout (above) so that the file output will have desired name
% change SERS sample input this is the text file from the microscope
% open the .txt file and put a 1 in for the first row. this balances the rows and column.
The program will not work if you do not do this.
%%%%%%%%%%%%%

org1  = load ('spec1.txt'); % non-sers
org2  = load ('spec4-2.txt');% sers
Sorg1 = load ('spec2.txt'); % non-sers _ standard
Sorg2 = load ('spec8-1.txt'); % sers _ standard

%-------------------------------------------------------------------------------
                     %-- Concentrations of the samples --%
%-------------------------------------------------------------------------------
cCVsamp     = 0.001;       % (M)
cCVsers     = 10.0e-8;      % (M)
cRef        = 8.76;        % (M)
%-------------------------------------------------------------------------------

%%%%%%%%%%%%%%%%%%%%%%%%%%%%%%%%%%%%%%%%%%%%%%%%%%%%%%%%%%%%%%%%%%%%%%%%%%%%%%%%
%---------------------------- dye integrate peaks ------------------------------%
%%%%%%%%%%%%%%%%%%%%%%%%%%%%%%%%%%%%%%%%%%%%%%%%%%%%%%%%%%%%%%%%%%%%%%%%%%%%%%%%

%-------------------------------------------------------------------------------%
 % ------------------ Normalize cvSAMP (calculate peak area) ------------------ %
%-------------------------------------------------------------------------------%


xorg = org1(:,1); x = xorg;
yorg = org1(:,2); y = yorg;

               cr = [6 73 134 314 538 605 909 1000];
                p = polyfit(x(cr),y(cr),6);
              fit = polyval(p,x);
            basey = y - fit;
```

```
 hold on
 plot(y);
 plot(fit);
 plot(basey);
 hold off
%axis([500 2500 -500 50000])
%return
clf
   cvSAMParea(1,1) = sum(basey(698:787));
   cvSAMParea(1,2) = sum(basey());
z=1
 % ------------------ Normalize cvSTAND (calculate peak area) ------------------ %

Sxorg = Sorg1(:,1);x = Sxorg;
Syorg = Sorg1(:,2);y = Syorg;
                cr = [1 38 257 417 638 712 857 1008];
                 p = polyfit(x(cr),y(cr),5);
               fit = polyval(p,x);
             baseS = y - fit;
       cvSAMPstarea = sum(baseS(480:540));

hold on
plot(y);
plot(fit);
plot(baseS);
hold off
%axis([350 650 -5000 50000])
%return
clf
z=2
%%%%%%%%%%%%%%%%%%%%%%%%%%%%%%%%%%%%%%%%%%%%%%%%%%%%%%%%%%%%%%%%%%%%%%%%%%%%%%%%%%
%%%%%%%%%%%%%%%%%%%%%%%%%%%%%%%%%%%%%%%%%%%%%%%%%%%%%%%%%%%%%%%%%%%%%%%%%%%%%%%%%%
%------------------------------------- -S-E-R-S- ---------------------------------%
%%%%%%%%%%%%%%%%%%%%%%%%%%%%%%%%%%%%%%%%%%%%%%%%%%%%%%%%%%%%%%%%%%%%%%%%%%%%%%%%%%
%%%%%%%%%%%%%%%%%%%%%%%%%%%%%%%%%%%%%%%%%%%%%%%%%%%%%%%%%%%%%%%%%%%%%%%%%%%%%%%%%%

%--------------------------------------------------------------------------------%
 % ------------------ Normalize cvSERS (calculate peak area) ------------------ %
%--------------------------------------------------------------------------------%

[nspec,npts] = size(org2);
        yorg = org2(2:nspec,:);
        xorg = org2(1,:);

           x = xorg;
           y = yorg;

% Loop To Normalize Each SERS Spectra %
% The 'j' loop is used to average 11 points so that the amount of error in each baseline
point might better represent (since there is alot of high frequency noise) the acutal
point intended.
clear basey
      [nspec,npts] = size(y);
                cx = [6 73 151 192 267 296 439 500 600 682 784 873 1000];
              [junk,slect] = size(cx);    % (1x13)
                 for i = 1:13;
                        cy(i,:) = cx(:,i)-5:cx(:,i)+5;
                 end
clear j
%plot(y(30,:));
for i = 1:nspec;
              spec = y(i,:);             % (601x1025)
                [npts,junk] = size(cy);  % (13x11)
                      for j = 1:npts;
                           specy(1,j) = mean(spec(cy(j,:))); % (1x13)
                       end
                 p = polyfit(x(cx),specy,4);
               fit = polyval(p,x);
```

```
            basey = spec - fit;
   cvSERSarea(i,1) = sum(basey(294:419));
   cvSERSarea(i,2) = sum(basey(698:787));
end
%return
 hold on
 plot(spec);
 plot(fit);
 plot(basey);
 hold off
%axis([350 650 -5000 50000]);
%return
clf
z=3
%-------------------------------------------------------------------------------%
 % ----------------- Normalize Standard (calculate peak area) ----------------- %
%-------------------------------------------------------------------------------%
[npts,axis] = size(Sorg2);
       Sxorg2 = Sorg2(:,1);
       Syorg2 = Sorg2(:,2);
           x = Sxorg2;
           y = Syorg2;
% ------- Loop To Normalize Each Standard Spectrum (calculate peak area) ------- %
      [nspec,npts] = size(y);
                cr = [50 100 150 200 250 300 350 472 600 650 700 750 800 850 900];
                 p = polyfit(x(cr),y(cr),3);
               fit = polyval(p,x);
             baseS = y - fit;
       cvSERSstarea = sum(baseS(450:575));
  hold on
  plot(y);
  plot(fit);
  plot(baseS);
  hold off
%return
clf
z=4
%%%%%%%%%%%%%%%%%%%%%%%%%%%%%%%%%%%%%%%%%%%%%%%%%%%%%%%%%%%%%%%%%%%%%%%%%%%%%%%
%%%%%%%%%%%%%%%%%%%%%%%%%%%%%%%%%%%%%%%%%%%%%%%%%%%%%%%%%%%%%%%%%%%%%%%%%%%%%%%
%------------------------ User Input For EF Calculations -------------------------%
%%%%%%%%%%%%%%%%%%%%%%%%%%%%%%%%%%%%%%%%%%%%%%%%%%%%%%%%%%%%%%%%%%%%%%%%%%%%%%%
%%%%%%%%%%%%%%%%%%%%%%%%%%%%%%%%%%%%%%%%%%%%%%%%%%%%%%%%%%%%%%%%%%%%%%%%%%%%%%%
% Equation
% (DthetaRS/domega)sample = (DthetaRS/domega)Ref x [Isamp/Iref] x [Cref/Csamp]


DXSref = 5.4*10^(-30); % Absolute differential cross section of the reference

%-------------------------------------------------------------------------------%
%%%%%%%%%%%%%%%%%%%%%%%%%%%%%%%%%%%%%%%%%%%%%%%%%%%%%%%%%%%%%%%%%%%%%%%%%%%%%%%
%------------------------------ Calculations -----------------------------------%
%%%%%%%%%%%%%%%%%%%%%%%%%%%%%%%%%%%%%%%%%%%%%%%%%%%%%%%%%%%%%%%%%%%%%%%%%%%%%%%
%-------------------------------------------------------------------------------%
                          %-- Diff Xsect sample --%
                        [nspec,npeaks] = size(cvSAMParea); %(1x2)
for i = 1:nspec;
  for j = 1:npeaks;
   CvDXSsamp(i,j) = (DXSref)*(cvSAMParea(i,j)/cvSAMPstarea)*(cRef/cCVsamp);
  end
end
z=5
%-------------------------------------------------------------------------------%
                          %-- Diff Xsect SERS --%
                         [nspec,npeaks] = size(cvSERSarea); %(1201x2)
for i = 1:nspec;
  for j = 1:npeaks;
    CvDXSsers(i,j) = (DXSref)*(cvSERSarea(i,j)/cvSERSstarea)*(cRef/cCVsers);
  end
```

```
end
z=6
%-------------------------------------------------------------------------------%
                              %-- SMEF For Dye --%
                                [ns,np] = size(cvSAMParea); %(1x2)
                           [nspec,npeaks] = size(cvSERSarea); %(1201x2)
for i = 1:nspec
  for j = 1:npeaks
    SMEFcv(i,j) = (CvDXSsers(i,j))/(CvDXSsamp(1,j));
  end
end

z=7
%-------------------------------------------------------------------------------%
hold on
plot(SMEFcv(:,1),'color',[1 0 0],'linewidth',lw);
plot(SMEFcv(:,2),'color',[1 0 0],'linewidth',lw);
hold off
xlabel('Spectral Repititions At 0.05 s Acquisition Time','fontsize',fs);
ylabel('SERS Enhancement Factor for CV at 10 nM','fontsize',fs);

print(fres,ftype,fileout);
return
```

Code ends here.

APPENDIX C. RAMAN DATA

This data was acquired with a 3 second integration time with 50 averages. The CV dye concentrations are listed in the charts below in nM with the associated SERS substrate. The spectra were baseline corrected before being fitted with a pseudo-Voigt function. The residuals of the fit are shown below the figure. The peak areas under the 804 and 918 cm^{-1} bands were extracted and used to calculate the AEF using equation 10.

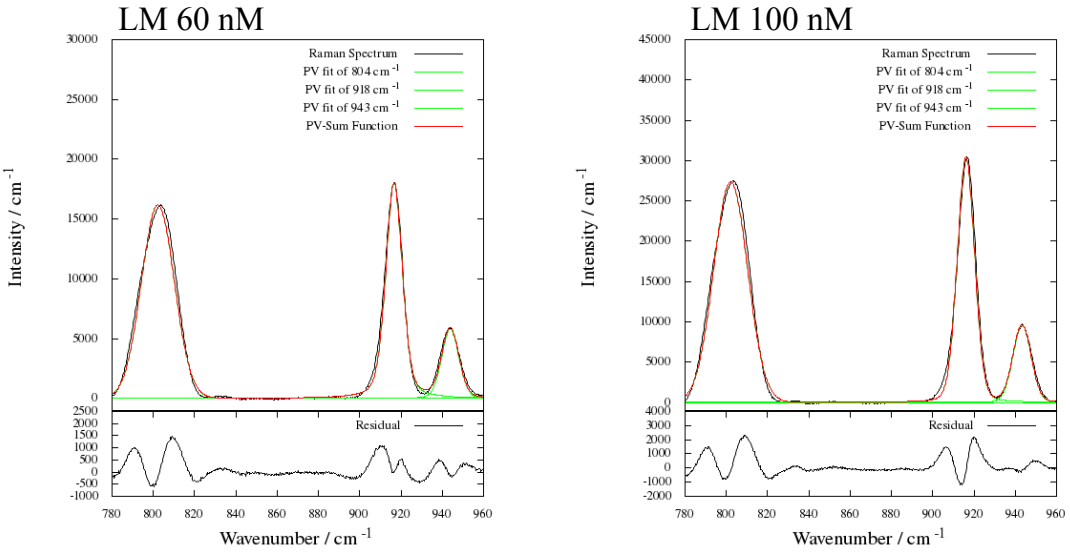

CV 1 mM

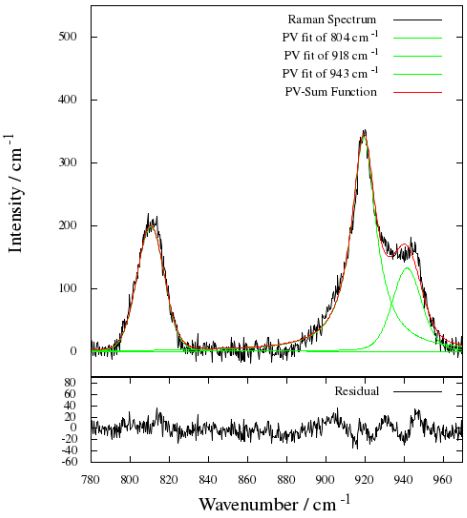

CV 1 mM

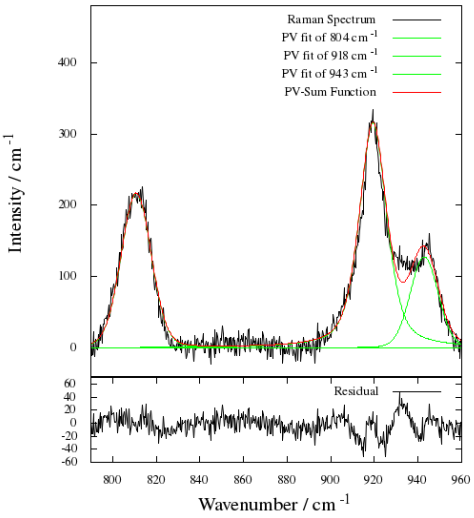

C4 50 nM

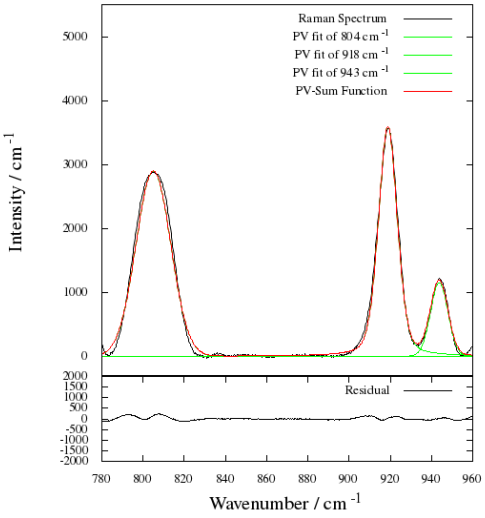

C4 100 nM

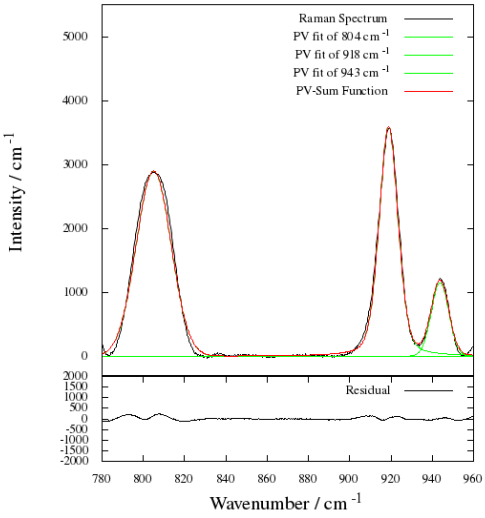

C3 50 nM

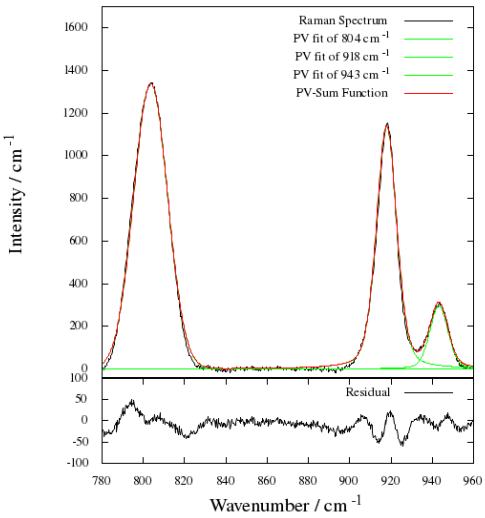

C3 100 nM

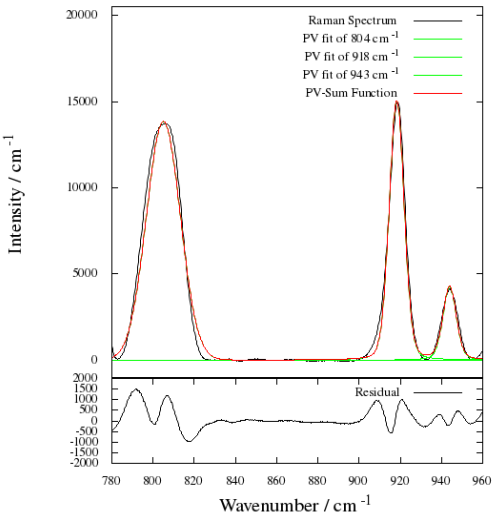

C2 50 nM

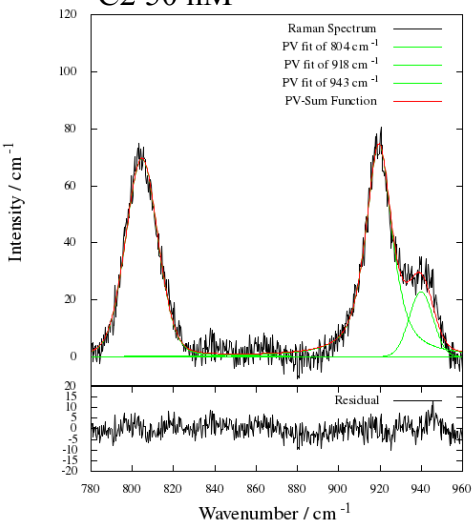

C2 100 nM

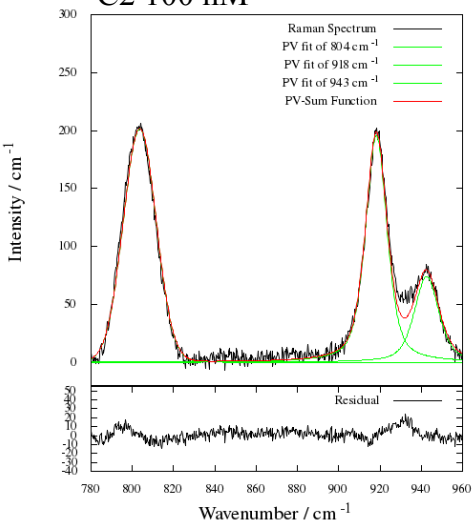

B4 50 nM

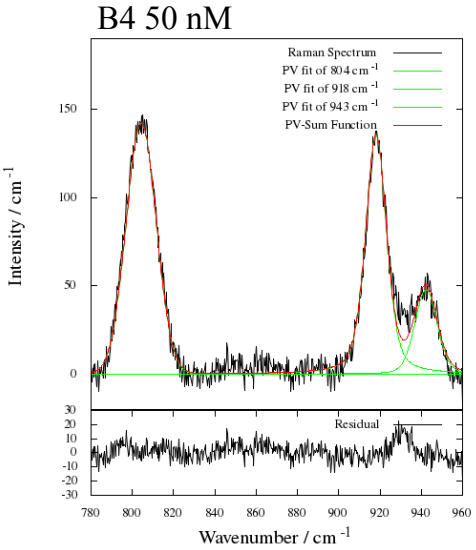

B3 100 nM

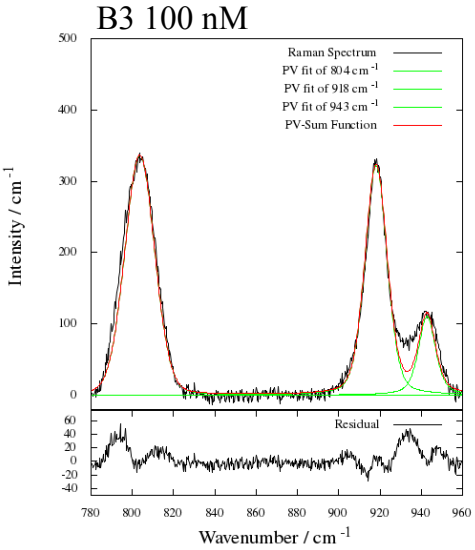

B2 50 nM

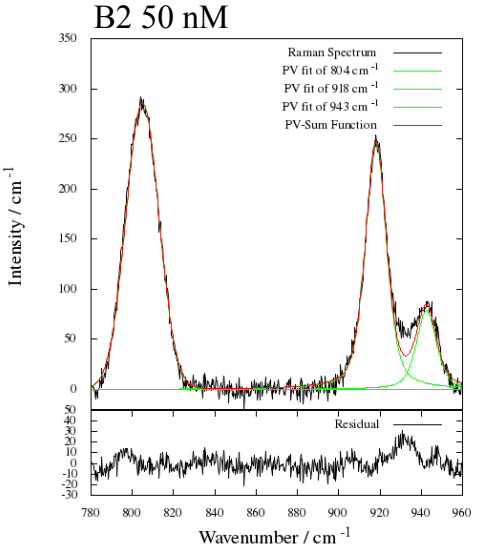

B2 100 nM